Quantum Transport

16

16.1 Quantum Transport

16.1.1 The Concept of Current in Quantum Mechanics

We have seen in Sect. 16.2.1 how we could define current in classical Drude theory in terms of electrons or charges obeying Newton's law with frictional forces giving rise to resistance. In Chap. 4 we had introduced the methodology of quantum mechanics and argued that classical physics was not really the right way of looking at dynamics on a microscopic scale. In practice it turns out that the classical theory of transport is very useful indeed, and one can go a long way in understanding transport phenomena in solid-state physics and engineering using the classical method. But there comes a point beyond which the classical description does not work well anymore, and we have to consider the quantum mechanical aspects. This happens on many occasion most of which we cannot discuss here, but we can consider a very simple and common situation where quantum mechanics is needed. Consider a beam of electrons injected, for example, in the conduction band of a semiconductor via an electrode and traveling to the other electrode. Now we can ask what is the current? In classical physics, the answer is obvious if we know the velocity of the carriers. Now we can insert a potential barrier on the way, for example, a material with a higher bandgap as in Fig. 16.1, and ask: what is the resistance produced by the potential barrier on the electrons impinging on it? A classical Drude approach would obviously give us a totally oversimplified and misleading answer to this question. It would require the definition of "frictional force" but which acts only in the form of one obstacle and would not give a satisfactory picture of this well-defined and concrete transport problem. So the right starting point in this case is the *quantum mechanical definition of the current (quantum current)*. To do this, and for simplicity, we consider a one-dimensional situation and write down the continuity equation:

M. Razeghi, *Fundamentals of Solid State Engineering*,
https://doi.org/10.1007/978-3-319-75708-7_16

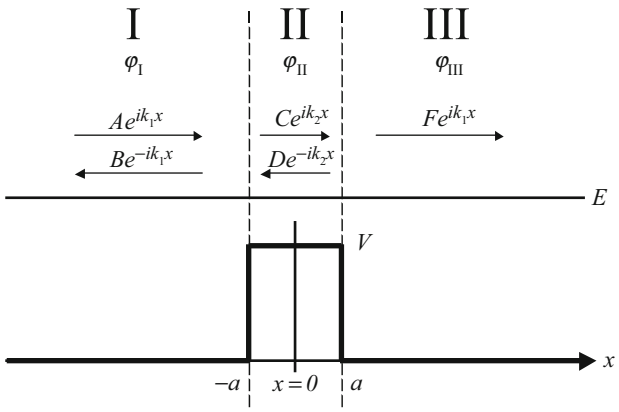

Fig. 16.1 Illustration of the three regions of particle motion

$$\frac{\partial \rho}{\partial t} + \frac{\partial J_x}{\partial x} = 0 \tag{16.1}$$

This equation is generally valid and is an expression of particle conservation where ρ is the density and J_x the current in x-direction. Now we rewrite the equation using the quantum mechanical definition of density and the time-dependent Schrödinger equation from Eq. (4.2). Recall that density in quantum mechanics is $\rho = \Psi^*\Psi$:

$$\frac{\partial(\Psi^*\Psi)}{\partial t} = \Psi^*\frac{\partial \Psi}{\partial t} + \Psi\frac{\partial \Psi^*}{\partial t} = \Psi^*\left(\frac{-i\,\widehat{H}}{\hbar}\Psi\right) + \Psi\left(\frac{i\,\widehat{H}}{\hbar}\right)\Psi^* \tag{16.2}$$

With the Hamiltonian:

$$\widehat{H} = \frac{p^2}{2m} + V(x) \tag{16.3}$$

Substituting the Hamiltonian from Eq. (16.3) into Eq. (16.2), we note that the potential energy term cancels and we have in one dimension:

$$\frac{\partial(\Psi^*\Psi)}{\partial t} = \frac{i\hbar}{2m}\left(\Psi^*\left(\nabla^2\Psi\right) - \Psi\left(\nabla^2\Psi^*\right)\right) \tag{16.4}$$

$$\frac{\partial(\Psi^*\Psi)}{\partial t} + \frac{\partial}{\partial x}\frac{\hbar}{2mi}\left(\Psi^*\left(\frac{\partial}{\partial x}\Psi\right) - \Psi\left(\frac{\partial}{\partial x}\Psi^*\right)\right) = 0 \tag{16.5}$$

From which it follows with Eq. (16.1):

$$J_x = \frac{\hbar}{2mi}\left(\Psi^* \frac{\partial \Psi}{\partial x} - \Psi \frac{\partial \Psi^*}{\partial x}\right) \tag{16.6}$$

This, Eq. (16.2), is the quantum mechanical definition of the current. It has some very interesting features. We note that it immediately follows that to carry a current, a wavefunction must be complex. In a closed system like a box, and in the absence of a magnetic field, i.e., when we have time reversal invariance, the wavefunction can always be chosen as real, and therefore the current is zero. This statement may not seem surprising perhaps, but it is very important. A plane wave e^{ikx}, for example, carries an electron current density of $-q\hbar k_x/m$ in the positive x-direction. So a beam of particles impinging from the left to right can be represented by such plane waves. Now consider what happens when a barrier is inserted in the path of such a beam. Clearly some will be reflected back, and some will go through the barrier. The question is how many per second will make it through? Classically only charges with sufficient energy to cross the barrier can go through. The quantum mechanical picture is quite different. This is one situation where one can see that the classical method does not work at all. So let us consider the quantum mechanical solution.

16.1.2 Transmission and Reflection Coefficients

Consider the diagram in Fig. 16.1 showing what happens to a beam of carriers impinging on a potential barrier.

We let a beam of particles come in from the left with amplitude A, and because some carriers will be reflected back again, there is a reflected beam with amplitude R traveling in the opposite direction. To the right of the barrier, there are no particles coming from the right, so there is a transmitted beam with amplitude F (Fig. 16.1). The potential regions are divided as follows:

$$\text{Region I} : x < -a, V = 0 \tag{16.7}$$

$$\text{Region II} : -a \leq x \leq +a, V > 0 \tag{16.8}$$

$$\text{Region III} : a < x, V = 0 \tag{16.9}$$

We also assume that the processes take place without the particles changing their energy. This is an example of "elastic scattering." So the solution of the time-dependent Schrödinger equation as defined in Chap. 4, Eq. (4.6), in each of the three regions can be written as:

$$\varphi_{\text{I}} = Ae^{ik_1 x} + Be^{-ik_1 x} \rightarrow E = \frac{\hbar^2 k_1^2}{2m} \tag{16.10}$$

$$\varphi_{\mathrm{II}} = C\mathrm{e}^{ik_2x} + D\mathrm{e}^{-ik_2x} \rightarrow E - V = \frac{\hbar^2 k_2^2}{2m} \tag{16.11}$$

$$\varphi_{\mathrm{III}} = Fe^{ik_1x} \rightarrow E = \frac{\hbar^2 k_1^2}{2m} \tag{16.12}$$

The transmission and reflection coefficients are defined by the relations:

$$T = \left|\frac{F}{A}\right|^2 \tag{16.13}$$

$$R = \left|\frac{B}{A}\right|^2 \tag{16.14}$$

To solve the problem, we now use the boundary conditions, continuity of the wavefunction, and its derivative, at $x = a$ and $x = -a$, to determine the coefficients. This gives four equations:

$$\mathrm{e}^{-ik_1a} + \frac{B}{A}\mathrm{e}^{ika_1} = \frac{C}{A}\mathrm{e}^{-ik_2a} + \frac{D}{A}\mathrm{e}^{ik_2a} \tag{16.15}$$

$$k_1\left[\mathrm{e}^{-ik_1a} - \frac{B}{A}\mathrm{e}^{ika_1}\right] = k_2\left[\frac{C}{A}\mathrm{e}^{-ik_2a} - \frac{D}{A}\mathrm{e}^{ik_2a}\right] \tag{16.16}$$

$$\frac{C}{A}\mathrm{e}^{ik_2a} + \frac{D}{A}\mathrm{e}^{-ik_2a} = \frac{F}{A}\mathrm{e}^{ik_1a} \tag{16.17}$$

$$k_2\left[\frac{C}{A}\mathrm{e}^{ik_2a} - \frac{D}{A}\mathrm{e}^{-ik_2a}\right] = k_1\frac{F}{A}\mathrm{e}^{ik_1a} \tag{16.18}$$

Solving these equations allows us to write:

$$\frac{F}{A} = \mathrm{e}^{-2ika_1}\left[\cos(2k_2a) - \frac{i}{2}\left(\frac{k_1^2 + k_2^2}{k_1k_2}\right)\sin(2k_2a)\right]^{-1} \tag{16.19}$$

$$2\frac{B}{A} = i\left(\frac{F}{A}\right)\frac{k_2^2 - k_1^2}{k_1k_2}\sin(2k_2a) \tag{16.20}$$

Using the relation:

$$\left(\left|\frac{F}{A}\right|^2 + \left|\frac{B}{A}\right|^2\right) = T + R = 1 \tag{16.21}$$

Which expresses the conservation of probability, we can find the transmission coefficient:

$$T = \frac{1}{1 + \frac{1}{4}\left(\frac{k_1^2 - k_2^2}{k_1 k_2}\right) \sin^2(2k_2 a)} \tag{16.22}$$

Or in terms of the energy E of the particle we have in the region $E > V$:

$$T = \frac{1}{1 + \frac{1}{4}\frac{V^2}{E(E-V)} \sin^2(2k_2 a)} \rightarrow E > V \tag{16.23}$$

where $k_2 = \sqrt{2m(E - V)/\hbar^2}$. The solution is still valid when $E < V$. Since k_2 is now complex, it is convenient to redefine:

$$ik_2 = \kappa \rightarrow \frac{\hbar^2 \kappa^2}{2m} = V - E > 0 \tag{16.24}$$

We can rewrite the transmission coefficient in this regime as:

$$T = \frac{1}{1 + \frac{1}{4}\frac{V^2}{E(V-E)} \sinh^2(2\kappa a)} \rightarrow E < V \tag{16.25}$$

The limit $E = V$ is of some interest. Taking this limit in Eq. (16.25) gives us:

$$T = \frac{1}{1 + \frac{2m(a)^2 V}{\hbar^2}} \rightarrow E = V \tag{16.26}$$

which shows that even when the kinetic energy is exactly as large as the potential energy, the transmission coefficient $T < 1$. Now consider a really interesting situation, namely, when $E > V$ and when in Eq. (16.23), we have the condition:

$$\sin^2(2k_2 a) = 0 \tag{16.27}$$

This happens when:

$$2ak_2 = n\pi \rightarrow n = 1, 2, 3 \ldots \tag{16.28}$$

With this condition it is equivalent to saying that when $2a = n\left(\frac{\lambda}{2}\right)2$, the transmission $T = 1$, i.e., we have a perfect transmission despite the fact that the particle has to cross an obstacle, and space is no longer homogeneous. At these resonance the particle does not see the scattering object. It behaves as if it were not there at all. The same phenomenon happens in optics for light transmission through a Fabry-Perot mirror at resonance. The requirement for perfect transmission can be rewritten as:

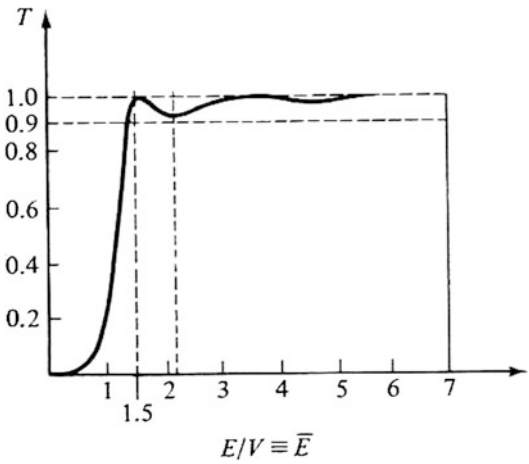

Fig. 16.2 Transmission coefficient for the single-barrier problem as a function of dimensionless energy (Reprinted with permission of Addison Wesley, R. Liboff "Quantum Mechanics, 2nd Edition" p. 231 Fig. 7.26, copyright Addison Wesley, 1992)

$$E - V = n^2 \left(\frac{\pi^2 \hbar^2}{8a^2 m} \right) \tag{16.29}$$

The behavior is shown in Fig. 16.2. When we have more than one barrier, or well, the above procedure is extended to allow reflected and transmitted waves in every region in the regions between the obstacles in a very natural generalization of the above example. In the two barrier case we have four unknown coefficients instead of two, but we have an extra boundary with two conditions.

16.1.3 Discussion

When considering the Quantum mechanical problem of transmission of particles through potential barriers, one can see a rich variety of behavior. This is true even for the simple problem of the transmission through a constant barrier as shown above. One of the most important results is the fact that one can transmit through a barrier even if one does not have enough kinetic energy to surmount it classically. This is a consequence of Heisenberg's uncertainty relation in which the delimitation of an obstacle in a specific region of space introduces indeterminance of momentum and energy. As the beam of particles is used to "measure" the presence of the object in a specific location, it no longer has a well-defined energy when it crosses the obstacle.

The transmission coefficient is, as one would expect, also a measure of the resistance or the conductance of the system. Let us examine what this implies for conductivity.

Fig. 16.3 Illustration showing the assumption that the charge reservoir on the right is shifted down by eV and that the electric field is not affecting the band structure of the system

16.1.4 The Electrical Resistance Due to Potential Barriers in Quantum Mechanics

We can consider this particle beam as being emitted from an electron reservoir in a metal and collected in a similar reservoir at a lower Fermi energy or chemical potential. So now we have the total current emitted from left to right which is (A = area, $2\ W$ = bandwidth, g_V = density of states per volume):

$$I_R = Ae \int_{-W}^{W} f(\varepsilon_k) g_V(\varepsilon_k) T(\varepsilon_k) \left(\frac{\hbar k_x}{m}\right) d\varepsilon_k \tag{16.30}$$

But from right to left, with carriers emitted from a reservoir held at a lower chemical potential of magnitude eV (see the drawing of Fig. 16.3), the current is:

$$I_L = Aq \int_{-W}^{W} f(\varepsilon_k + qV) g_V(\varepsilon_k) T(\varepsilon_k) \left(\frac{\hbar k_x}{m}\right) d\varepsilon_k \tag{16.31}$$

The net current is therefore the difference which is:

$$I_R = Aq \int_{-W}^{W} \{f(\varepsilon_k) - f(\varepsilon_k + qV)\} g_V(\varepsilon_k) T(\varepsilon_k) \left(\frac{\hbar k_x}{m}\right) d\varepsilon_k \tag{16.32}$$

For small voltages we can expand the Fermi function to order qV to obtain:

$$I = Aq^2 V \int_{-W}^{W} \left(-\frac{\partial f}{\partial \varepsilon_k}\right) g_V(\varepsilon_k) T(\varepsilon_k) \left(\frac{\hbar k_x}{m}\right) d\varepsilon_k \tag{16.33}$$

This elegant result shows how the transmission coefficient determines and defines the conductance G of the system which is:

$$G = Aq^2 \int_{-W}^{W} \left(-\frac{\partial f}{\partial \varepsilon_k}\right) g_V(\varepsilon_k) T(\varepsilon_k) \left(\frac{\hbar k_x}{m}\right) d\varepsilon_k \tag{16.34}$$

And we should remember that at $T = 0$, the derivative of the Fermi function is a delta function at the Fermi level so that $G = Aq^2 g_V(\varepsilon_F) T(\varepsilon_F) v(\varepsilon_F)$ where $v(\varepsilon_F)$ is the Fermi level velocity $v_F = \sqrt{2E_F/m}$.

This result is now easily generalized to multiples of barriers of various shapes and sizes. In all cases, we need to calculate the new transmission coefficient using the generalization of the same method.

The above derivation assumed free electrons. For band electrons the x-velocity should be replaced by $\frac{1}{\hbar}\frac{\partial \varepsilon_k}{\partial k_x}$, and the mass is the effective mass m^*.

The reader will note that if Eq. (16.34) is compared to the classical Drude result, then it is possible to define an effective Drude relaxation time via the relation $\{\sigma_{\text{Drude}} = \frac{nq^2\tau}{m^*},\ g_V(\varepsilon_F)\varepsilon_F = n\}$:

$$\tau = \frac{2TL}{v(\varepsilon_F)} \tag{16.35}$$

Note that the Drude relaxation time scales as length times $T(E_f)$. Indeed in a macroscopic resistor $T(L)$ will depend on the number of obstacles and also change, decreasing with L. If we assume that the wavefunction loses its coherence each time after scattering from an obstacle, then every time it crosses an obstacle, it is like starting again at the next one, then the resistance caused by each obstacle is additive, and the scaling of T will be as $1/L$, $1/T = \sum_n 1/T_n = \frac{L}{w} < \frac{1}{T_n} >$ where w is the average distance between the obstacles so that:

$$\tau = \frac{2\left\{< T_n^{-1} >\right\}^{-1} w}{v(\varepsilon_F)} \tag{16.36}$$

Where $<>$ = average denotes the average over the distribution of T_n. On the other hand if the system is ordered, and the total transmission coefficient does not change with L, and stays at $T = 1$, we can see that the Drude relaxation time goes to infinity with L, so that the resistivity of the macroscopic material tends to zero.

16.1.5 The Influence of the Applied Electric Field

We have up to now not mentioned the electric field. By drawing the transport path as in Fig. 16.4, we have avoided the problem of having to mention the applied electric field altogether. The only reason why there is a current is because the electrons in the right reservoir have a lower Fermi level, so the number crossing from left to right for

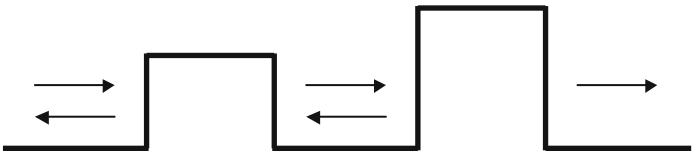

Fig. 16.4 The diagram illustrates a two barrier path with different barrier heights. The methodology of the solution is as before

a given temperature is smaller. But in reality there is, of course, an electric field gradient and electrons emitted to the right are subject to a field, and classically, they are accelerated by this field and then they scatter and/or just reach the other electrode. The quantum mechanical problem of a charge moving in an electric field was treated in Chap. 10. The problematic is not as simple as in classical physics because we deal with energy eigenstates not with acceleration and instantaneous velocities. So we avoided this issue at this stage, and it is all right to do so provided the applied potential is small, and we can work in the linear response or ohmic regime keeping only terms in first order in the applied potential. From Eq. (16.33) we observe that to linear order in V, the transmission coefficient and wavefunctions use to do derive it can be assumed to be the zero field values. So here we have neglected the fact that the field will change the energy levels, that these energy levels will have a spatial structure as treated in Sect. 16.2.1, that consequently the electrons can also relax their energy to the lattice as they move, and that there is energy dissipation or joule heating in going from left to right. The energy relaxation steps do also lead to resistance processes, but in many situations of interest in quantum devices, the barrier reflections and tunneling processes where energy is conserved are by far more important for resistance than the energy exchange with the lattice.

16.1.6 Resonant Tunneling Over a Double Barrier

Let us now consider the double barrier obstacle as shown in Fig. 16.5. In the zero-bias limit, the diagram shows the position of the Fermi level of the reservoirs by the dashed line and the two quantum well eigenstate E_0 and E_1. The application of a bias field changes the potential profile. As shown, as soon as the bias is big enough for the E_0 level to line up with the injecting Fermi level, we have the phenomenon of resonance. The incoming energy exactly matches the quantum well energy, and we have an enhanced transmission. The modeling of the transmission coefficient using the method outlined above is shown in Fig. 16.1 for two different values of well widths. One can clearly see how the current rises with bias reaches a maximum at resonance and when the injecting level and quantum well level move out alignment, the current decreases again and we have the phenomenon known as negative differential resistance (NDR). The phenomenon of transmission resonance can be understood very easily using the perturbation method of Chap. 4.

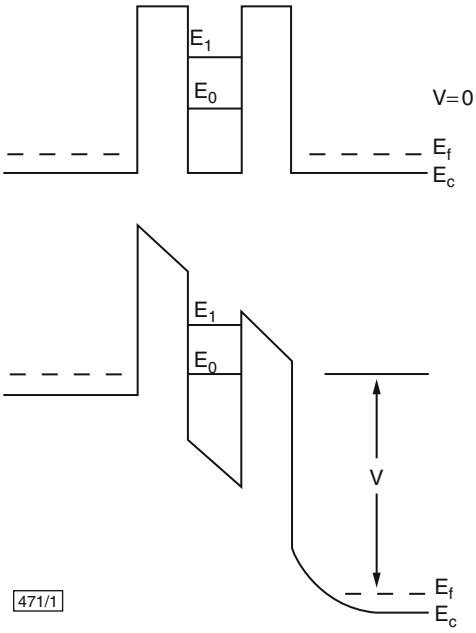

Fig. 16.5 The conduction-band profile for a double barrier resonant-tunneling structure (Copyright 1989 from "The MOCVD Challenge, Vol. 1: A Survey of GaInAsP-InP for Photonic and Electronic Applications," Razeghi, M., p. 114, Fig. 3.37. Reproduced with permission of Routledge/Taylor & Francis Group,LLC)

We consider the electron at the injector Fermi level uncoupled to the quantum well to be in the state $\phi_I(\varepsilon_F)$ and regions I and II as defined above in Eq. (16.7) to denote the left and right reservoirs; then we allow a coupling to the quantum well level state E_0, with strength t_{I0} similarly for E_1. Now by perturbation theory to first order in the coupling, the reservoir eigenstate will be admixed to the quantum well eigenstates to give (E_0, $E_1 > \varepsilon_F$):

$$\Psi = \phi_1(\varepsilon_F) + \frac{t_{I0}}{\varepsilon_F[I] - E_0}\phi_0 + \frac{t_{I1}}{\varepsilon_F[I] - E_1}\phi_1 \tag{16.37}$$

In the present of a bias, one can approximately assume that the couplings t and the quantum well levels change so that $E_{0,\,1} \to E_{0,\,1} - qFa$ where a is the first barrier width and F the applied field so that:

$$\Psi_I = \phi_1^0(\varepsilon_F) + \frac{t_{I0}(F)}{\varepsilon_F - E_0 + qFa}\phi_0 + \frac{t_{I1}(F)}{\varepsilon_F - E_1 + qFa}\phi_1 \tag{16.38}$$

Now we see that when the levels aligns, the admixture diverges, the wavefunction acquires a high probability of mixing with the quantum well state. Of course at resonance one has to use the degenerate state perturbation method also explained in Chap. 4. To evaluate the full transmission with this method, one has to allow the coupling to the second reservoir as well and then obtain the amplitude of the initial state in the final state. But this is straightforward. Experimentally one can observe these negative differential resistance resonances, but it is not a trivial task, and a

number of conditions have to be satisfied. The quantum well levels are in practice not just sharp eigenstates but they are subject to broadening in the plane specially if the semiconductor layers are highly doped. Note that the same perturbation procedure can be applied to the second reservoir, and thus one can couple the initial reservoir to the final reservoir by a simple extension of the above perturbation theory, i.e., replacing ϕ_0 with:

$$\phi_0 = \phi_0^0 + \sum_{\varepsilon_{\mathrm{II}}} \frac{t_{0\varepsilon}^{w}(F)}{E_0 - \varepsilon_{\mathrm{II}} + qFa} \phi_{\mathrm{II}}(\varepsilon) \tag{16.39}$$

where $\varepsilon_{\mathrm{II}}$ is now any energy in the final reservoir and $t_{0\varepsilon_{\mathrm{II}}}^{w}$ is the admixture energy from the zero energy state in the well w to the final energy in the right reservoir, or electrode II, and not just the Fermi level. When the carrier has arrived in the second reservoir, it still has the field energy which it has acquired on the way, and it can deposit it in the electrode. Similarly for the upper energy level in the central well. The scattering-induced broadening washes out some of the features as one might expect. For example, from Eq. (16.38), the broadening can be represented as an imaginary part contribution $i\Gamma$ to the energy which gives the admixture probability:

$$|a_{I0}|^2 = \frac{|t_{I0}|^2}{(\varepsilon_F - E_0 + qFa)^2 + \Gamma^2} \tag{16.40}$$

Then there is also the thermal broadening effects which we can also include in the broadening width, and the fact that off resonance, when the quantum inelastic tunneling transport paths are improbable, the carrier can cross the obstacle by using the thermal activation into the quantum well levels. The so-called phonon-assisted pathways are important as we go up in temperature. Figure 16.6 shows the

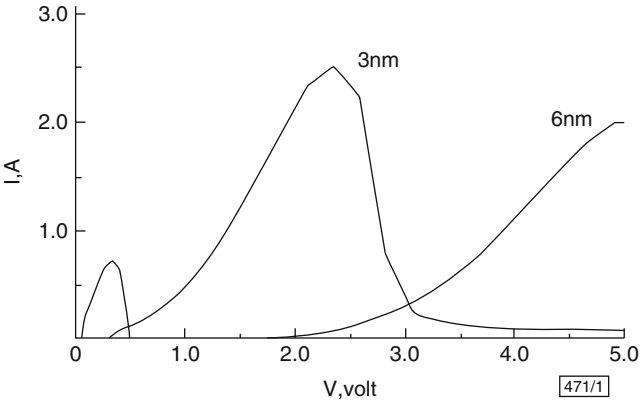

Fig. 16.6 Resonant-tunneling current/voltage simulations for 3- and 6-nm-wide wells (Copyright 1989 from "The MOCVD Challenge, Vol. 1: A Survey of GaInAsP-InP for Photonic and Electronic Applications," Razeghi, M., p. 114, Fig. 3.38. Reproduced with permission of Routledge/Taylor & Francis Group, LLC)

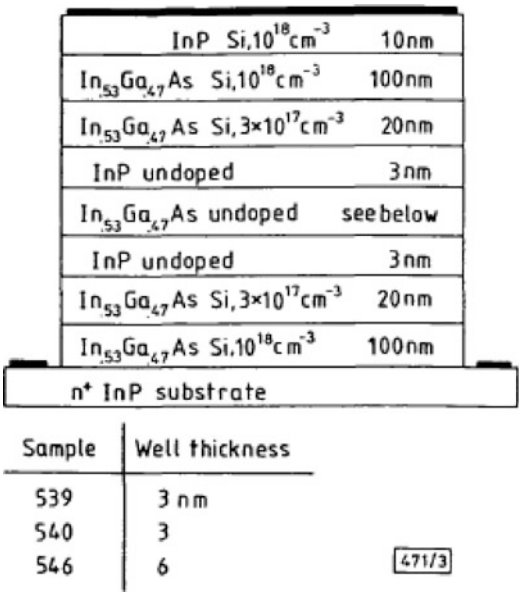

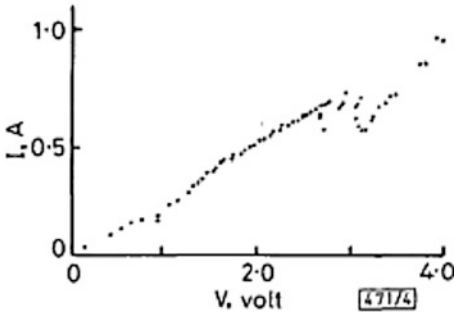

Fig. 16.7 The structure of the device used by Razeghi et al. in 1987 (Reprinted with permission from Electronics Letters Vol. 23, Razeghi, M., Tardella,A., Davis, R., Long, A., and Kelly, M., "Negative Differential Resistance at room temperature from resonant-tunneling GaInAS/InP double barrier structures," p. 116. Copyright 1987, IEEE)

Fig. 16.8 Pulsed current/voltage characteristic for a sample showing negative differential resistance at 3 V bias (Reprinted with permission from Electronics Letters Vol. 23, Razeghi, M., Tardella, A., Davi, R., Long, A., and Kelly, M., "Negative Differential Resistance at room temperature from resonant-tunneling GaInAS/InP double barrier structures," p. 116. Copyright 1987, IEEE)

calculated negative differential resistance in the device structure shown in Fig. 16.7. In Fig. 16.8 one can see the negative differential resistance obtained by a voltage pulsed technique at room temperature. The pulsing ensures that space charge and thus internal field effects do not mask the quantum tunneling process.

It is also possible to see negative differential resistance (NDR) in the steady state in some materials and especially if we go down to low temperatures where thermal

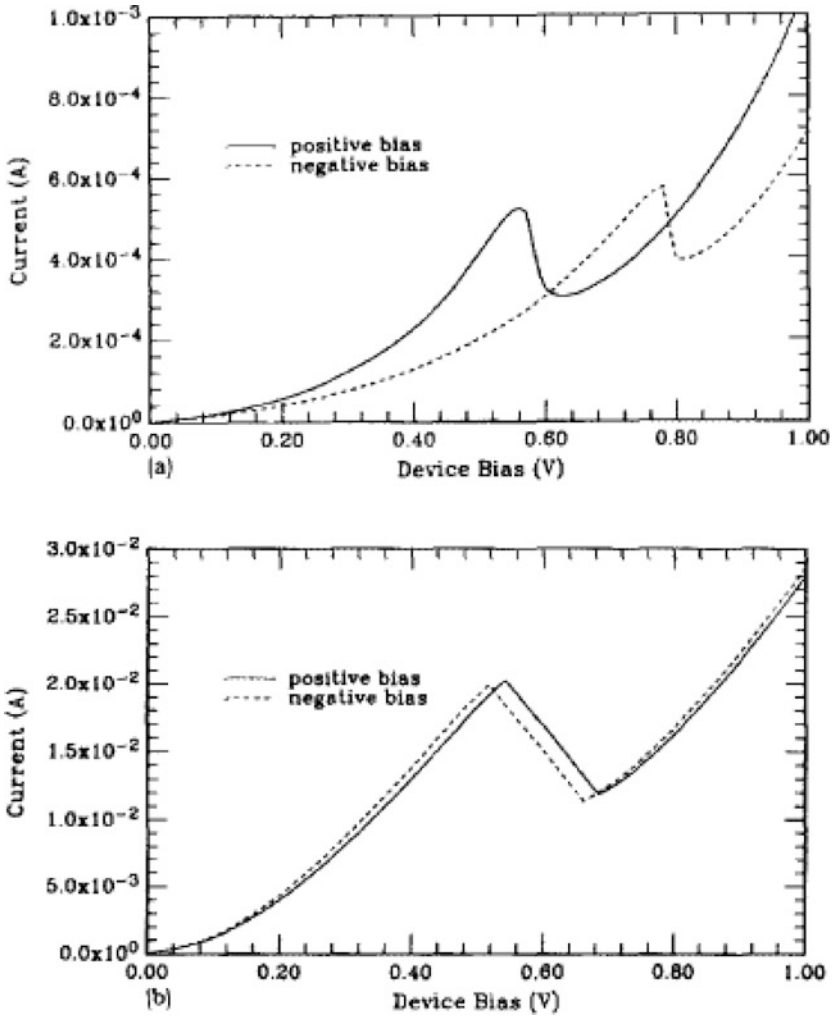

Fig. 16.9 Resonant tunneling through a double GaAs/AlAs superlattice barrier, single-quantum well heterostructure (Reprinted with permission from Applied Physics Letters Vol. 49, Reed, M., Lee, J., Tsai, H., "Resonant tunneling through a double GaAs /AlAs superlattice barrier single quantum well heterostructure," p. 158. Copyright 1986, American Institute of Physics)

broadening and pathways are suppressed. Figure 16.9 shows the NDR produced at room temperature in a GaAs/AlAs double barrier system.

The reader is referred to the books by M. Kelley and C. Weisbuch and B. Vinter for a more detailed review of negative differential resistance in quantum devices.

16.1.7 The Superlattice Dispersion

One of the most interesting phenomena of quantum physics is produced when we apply a strong electric field to narrow energy bands. The case of free electrons in an electric field was treated in Chap. 11, and there we were interested in what happens to the optical absorption in a semiconductor. Here we want to focus on what happens in narrow energy bands and show that the physics is very novel and interesting. Let us first recall the Kronig-Penney band structure of Chap. 5. This model is actually a very good representation of the band structure of a semiconductor superlattice as shown schematically in Fig. 16.10. A popular example considered in practically every specialized book (see Razeghi 1989; Weisbuch and Vinter 1991, Davis 2000, Kelly 2000) is the GaAs/AlAs superlattice.

With infinite barriers, the individual quantum wells would have confined eigenstates as shown in Fig. 4.7 in Chap. 4. When the barriers are finite, the quantum well confined levels can tunnel across and then overlap with each other thus forming energy band whose width can be adjusted as was done in the Kronig-Penney model in Sect. 16.2.1. In principle we can proceed as for the Kronig-Penney model here too. But there is a quicker way to examine the band structure specially when there is an electric field and that is to use the "tight binding model." In the framework of the tight-binding model discussed in Chaps. 1 and 5, the overlap or coupling between the confined levels of subband "n" in two adjacent wells can be written as:

$$\begin{aligned} t^n_{l,l+1} &= \int dz \Psi^*_{n,l} V(z)) \Psi_{n,l+1} \\ t_{l,l+1} &= t^*_{l+1,l} \end{aligned} \tag{16.41}$$

where Ψ is the confined quantum well state in well l, $V(z)$ is the potential caused by the adjacent well which starts at $z = a$ and finishes at $z = b$, and the superlattice distance is $c = \frac{a+b}{2}$ (see Fig. 16.10). The coupled Bloch wavefunction of energy E in one dimension can be written as a superposition of the individual quantum well (n subband) state:

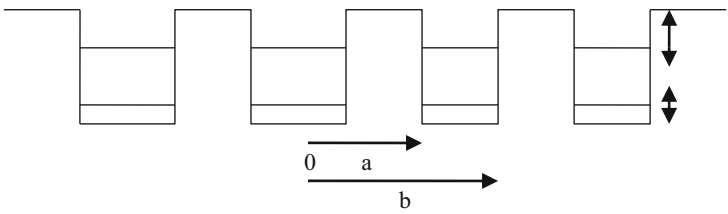

Fig. 16.10 The schematic representation of a superlattice periodic potential in the growth direction. The vertical arrows denote the expected width of the so-called superlattice minibands formed by the coupling of the quantum well wavefunctions as in the Kronig-Penney model of Sect. 16.2.1

$$\phi_E(z) = \sum_l C_l^n \Psi_{n,l} = \sum_l C_l^n |n,l\rangle \tag{16.42}$$

Taking the expectation value of the Hamiltonian with the coupled states, Eq. (16.42) gives by definition:

$$E = \langle \phi_E | H_0 + V | \phi_E \rangle \tag{16.43}$$

When substituting Eq. (16.42) into Eq. (16.43) and evaluating the right-hand side, we encounter terms of the form:

$$\langle n,l|H_0|n,l\rangle = E_n^0 \tag{16.44}$$

$$\langle n,l|H_0|n,l'\rangle \tilde{} 0 \rightarrow l \neq l' \tag{16.45}$$

$$\langle n,l|H_0|n',l\rangle = 0 \rightarrow n \neq n' \tag{16.46}$$

$$\langle n,l|V(z)|n,l\pm 1\rangle = t \tag{16.47}$$

$$\langle n,l|V(z)|l',n'\rangle \tilde{} 0 \rightarrow l' \neq l \pm 1, n \neq n' \tag{16.48}$$

The above relations give the following relations for the coefficients:

$$\begin{aligned} EC_l^n &= E_n^0 C_l^n + t_n\left(C_{l+1}^n + C_{l-1}^n\right) \\ t_{l,l\pm 1}^n &= t_n \end{aligned} \tag{16.49}$$

The equation can be solved by making use of the translational symmetry and Bloch's theorem which says that:

$$\begin{aligned} C_{l+1}^n &= C_l^n \mathrm{e}^{ik_z c} \\ C_{l-1}^n &= C_l^n \mathrm{e}^{-ik_z c} \end{aligned} \tag{16.50}$$

where c is the lattice repeat distance so Eq. (16.49) becomes:

$$\begin{aligned} \left(E - E_n^0 - 2t_n \cos k_z c\right) C_l^n &= 0 \\ E_n(k_z) &= E_n^0 + 2t_n \cos k_z c \end{aligned} \tag{16.51}$$

This cosine dispersion is a good approximation to the superlattice band structure in the growth direction. The wavefunctions in Eq. (16.49) are now labeled with the k_z vector as $\varphi_{n,kz}$.

16.1.8 The Stark-Wannier States

Now consider the application of an electric field in the z-direction. This introduces an extra term in the Hamiltonian, with F denoting the applied electric field:

$$H_F = H + qFz \tag{16.52}$$

Now we can expand the new eigenstates in terms of the new Bloch states we have just derived. For convenience, we only deal with z-component, the x,y directions are free electron effective mass states, and the total energy is decomposed as $E = E_z + \varepsilon(k_y) + \varepsilon(k_x)$

$$\Psi(z) = \sum_{n,k_z} A_n(k_z)\phi_{n,k_z}(z) \tag{16.53}$$

With $H_F\Psi(z) = E_z\Psi(z)$, we have after multiplying the left with using the orthogonality of the wavefunctions:

$$\left(E_z - E_{n,k_z}\right)A_n(k_z) = qF\sum_{k_z',j} Z_{n,k_z;j,k_z'}A_j\left(k_z'\right) \tag{16.54}$$

where:

$$Z_{n,k_z;j,k_z'} = \int dz\phi^*_{n,k_z}(z)z\phi_{j,k_z'}(z) \tag{16.55}$$

and the matrix elements Eq. (16.55) obey the rule:

$$Z_{n,k_z;j,k_z'} = i\delta_{n,j}\delta_{k_z,k_z'}\frac{\partial}{\partial k_z} \tag{16.56}$$

Substituting Eq. (16.56) back into Eq. (16.54) gives us a first-order differential equation:

$$\left(E_z - E_{n,k_z}\right)A_n(k_z) = iqF\frac{\partial A_n(k_z)}{\partial k_z} \tag{16.57}$$

which we can integrate straight away by first dividing throughout with A_n, to give after substitution Eq. (16.53):

$$\Psi_\nu{}^n(z) = \int_{-\pi/c}^{\pi/c} c^{1/2}\frac{dk_z}{2\pi}\exp\left[ik_z(z-\nu c) - \frac{it_n}{qFc}\sin k_z c\right] \tag{16.58}$$

where we have used the relations:

$$E_z = qFc\nu + E_n^0 \tag{16.59}$$

$$\sum_{k_z} \rightarrow \frac{L}{2\pi}\int dk_z \tag{16.60}$$

$$E_n(k_z) = E_n^0 + 2t_n \cos k_z c \tag{16.61}$$

This defines the energy levels. The Bloch symmetry in the superlattice which stipulates that the same functions must be reproduced if the origin is shifted to an equivalent site forces the indices ν to be integers ranging from $(-\infty, \infty)$. The complete wavefunctions and energies are now given by:

$$\Psi_E(x,y,z) = \int_{-\pi/c}^{\pi/c} c^{1/2}\frac{dk_z}{2\pi}\exp\left[ik_z(z-\nu c) - \frac{2it_n}{qFc}\sin k_z c\right] \times \left(\frac{1}{L_x L_y}\right)^{1/2}\exp\left(ik_x x + ik_y y\right) \tag{16.62}$$

$$E = qFc\nu + E_n^0 + \frac{\hbar^2}{2m^*}\left(k_x^2 + k_y^2\right) \rightarrow -\infty < \nu < \infty \tag{16.63}$$

The wavefunction in the z-direction is a well-known function in mathematical physics, and it is called the Bessel function of the first kind J and can be written in the usual way as:

$$\int_{-\pi/c}^{\pi/c} c\frac{dk_z}{2\pi}\exp\left[ik_z(z-\nu c) - \frac{it_n}{qFc}\sin k_z c\right] = J_{\frac{z}{c}-\nu}\left(\frac{2t_n}{qFc}\right) \tag{16.64}$$

The new physics is fascinating. The first thing we note is that the Bessel functions are localized in the z-direction. Starting from an origin νc, the wavefunction decays after a distance of L_n where

$$L_n = \frac{2t_n}{qF} \tag{16.65}$$

The stronger the electric field, the smaller the wavefunction. This is classically completely counterintuitive. The eigenstates will form a so-called Stark-Wannier (SW) ladder centered about the middle of every quantum well in the superlattice, extending to about the distance L_n in the z-direction. Since the banding parameter t_n increases as we go up in the quantum well subband index n, because the confinement is weaker at higher energies (see Chap. 4 Eq. (4.47)), the localization length of the Stark-Wannier states increases for the higher energy bands in the superlattice.

If an electron is put in any of the Stark-Wannier states, it is in an eigenstate and will stay there forever and not transport charge unless it is allowed to couple with the photon or phonon fields. And of course it is coupled to those fields, and thus it will relax down the Stark-Wannier energy ladder emitting light or heat as it moves. The current or drift velocity is then limited by the rate of energy relaxation. If we calculate this rate (Movaghar 1987), then we can calculate the drift velocity. If the energy relaxing coupling Hamiltonian is $H_r(z)$ then by the Fermi golden rule (see Chap. 10), we have the rate:

$$\begin{aligned}\gamma_{\nu\nu'} &= \frac{2\pi}{\hbar}\sum_s \left|\int dz \Psi_\nu^*(z) V_r(z,\omega_s)\Psi_{\nu'}\right|^2 \delta(qcF\nu' - qcF\nu + \hbar\omega_s)(1+n(\omega_s)) \\ &\quad \rightarrow qcF\nu > qcF\nu' \\ V_r(z,t) &= V_r(z,\omega_s)\mathrm{e}^{i\omega_s t} + V_r^*(z,\omega_s)\mathrm{e}^{-i\omega_s t}\end{aligned} \tag{16.66}$$

where the excitations ω_s emitted can be phonons or photons and V_r is the relaxation coupling. Even though the dominant relaxation channel is phononic, specially when there is a resonant Stark-Wannier transition with an optic phonon mode, the photons emission can be turned into a lasing emission in the so-called quantum cascade laser (QCL) structure (see Faist et al. 1994 and Slivken et al. 2002, in the further reading section for more information). In the process $\nu \rightarrow \nu'$ the distance traveled is $d = c(\nu' - \nu)$ which then defines a transfer velocity. Moving against the field is also possible but will involve an absorption of the excitation involved. But the excitation has to be available so the "up rate" involves an activation factor via the phonon or photon occupation number $n(\omega_s)$. Again from the Fermi golden rule for absorption going up the energy ladder, we have:

$$\begin{aligned}\gamma_{\nu\nu'} &= \frac{2\pi}{\hbar}\sum_s \left|\int dz \Psi_\nu^*(z) V_r(z,\omega_s)\Psi_{\nu'}\right|^2 \delta(qcF\nu - qcF\nu' + \hbar\omega_s)(n(\omega_s)) \\ &\quad \rightarrow qcF\nu' > qcF\nu\end{aligned} \tag{16.67}$$

$$n(\omega_s) = \frac{1}{(e^{\hbar\omega_s/k_bT} - 1)} \tag{16.68}$$

We conclude that the motion of electrons in finite energy bands in quantum mechanics gives rise to a very different physical picture than in classical physics. What is happening here viewed in the semiclassical picture is that the carriers are accelerated by the electric field to go up the Bloch band energy ladder (assume $t_n < 0$):

$$\frac{d\vec{k}}{dt} = -q\vec{F} \tag{16.69}$$

$$E_n(k) = E_n^0 - 2|t_n| \cos k(t)c \tag{16.70}$$

Since the energy is periodic, in the absence of energy dissipation, the electron accelerates and then slows down again when it reaches the top of the energy band and then actually has to return in space to move against the field. It cannot go further than a certain distance in space without losing energy, because its energy will have reached the top of the allowed energy band which is $E = E_n^0$. Its motion in energy space is periodic and so is its motion in real space. This motion is called Bloch oscillations, and one can understand that the particle is being actually localized by the applied field. In order to move a longer distance than the Stark-Wannier length, the carrier has to emit energy, and in the quantum mechanics point of view, relax down into the adjacent Stark-Wannier state or classically speaking, start a new journey forward in field direction in space as soon as it has emitted energy, thus avoiding to have to go back in space. The reason why the simple classical viewpoint is valid in many situations is that the electron has in most cases plenty of opportunity to relax its energy before it has reached the top of the band. In formal language, the energy relaxation time (inverse of the rate) is short compared to the time it takes to reach the top of the band via Eqs. (16.69) and (16.70). Under these circumstances it is possible to think of the relaxation as a frictional force acting on a carrier which remains in the effective mass regime staying in the small k region with $\cos kc \sim 1 - (kc)^2/2$.

16.1.9 Quantum Transport in Two-Dimensional Channels

One of the most brilliant discoveries of quantum well physics is the idea of the modulation-doped structure, shown on the right-hand side of Fig. 16.11 and more explicitly in Fig. 16.13. The dopant is introduced in the barrier layer as, for example, in Fig. 16.11 in the AlGaAs layer. In this way the carrier moves into the region of low energy which is the conduction band of the GaAs layer and leaves its counterion behind in the barrier. The counterion is now well separated in space from the conducting channel formed in parallel and shown in Fig. 16.13. The physical separation from the dopant means that the charge impurity scattering contribution is considerably reduced compared to the normal case.

The scattering rate can be written as:

$$\frac{1}{\tau_{\text{imp}}} = N_{\text{imp}} \frac{m^*}{2\pi\hbar^3 k_F^3} \left(\frac{q^2}{2\varepsilon_0 \varepsilon_b}\right) \int_0^{2k_F} \frac{\mathrm{e}^{-2k|d|}}{[k + q_I G(k)]^2} \left(\frac{b}{b+k}\right)^6 \frac{k^2}{\sqrt{1 - (k/2k_F)^2}} dk \tag{16.71}$$

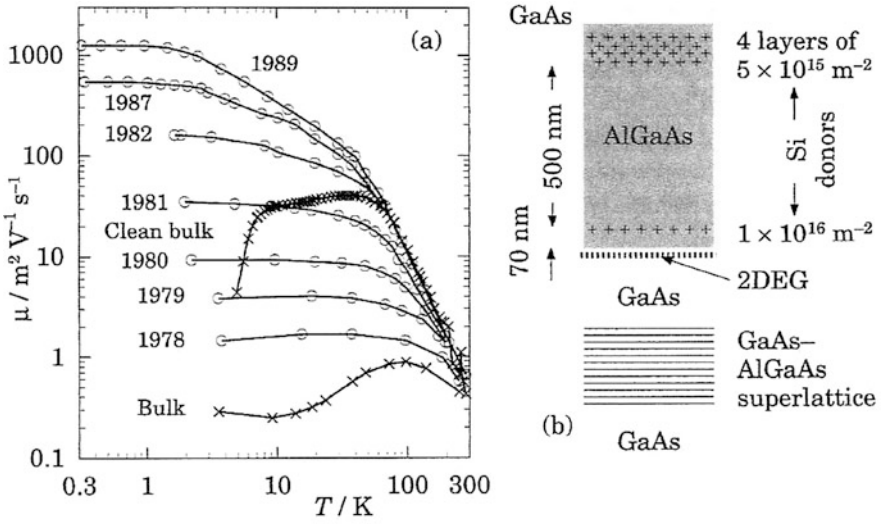

Fig. 16.11 Mobility of various two-dimensional electron gases 2DEGs as a function of temperature (circles) showing how the peak mobility which is limited by impurity scattering has increased over the 20 years shown. The mobility of bulk samples is shown for comparison (crosses) for older material (bulk) and newer material (clean bulk). On the right we see a simplified structure of a wafer grown in the sample of highest mobility (From J.H Davis "The physics of low dimensional semiconductors" p. 360, Fig. 9.11a, copyright Cambridge University press 1998, redrawn from Applied Physics Letters Vol. 55 "Electron mobilities exceeding 10^7 $cm^2/V{\cdot}s$ in modulation-doped GaAs," pg. 1888, Fig. 1, copyright American Institute of Physics 1989. Reprinted with permission of Cambridge University press and American Institute of Physics)

$$G(k) = \frac{1}{8}\left[2\left(\frac{b}{b+k}\right)^3 + 3\left(\frac{b}{b+k}\right)^2 + \left(3\frac{b}{b+k}\right)\right] \tag{16.72}$$

where b is defined below, N_{imp} and N_{2D} are the 2D-impurity and the 2D electron concentrations in the dopant layer, respectively, and d is the distance to the impurity dopant layer as measured from the edge of the GaAs layer (see Fig. 16.12); the remaining parameters are defined later (Fig. 16.13).

And the wavefunction in the channel (see Fig. 16.12) is plane wave like in (x,y) plane and in confined z-direction-given by (Ando et al. 1982):

$$u(z) = \left(\frac{b^3}{2}\right)^{1/2} z\exp[-bz/2] \tag{16.73}$$

b is the so-called Fang-Howard decay parameter given by:

$$b = \left(\frac{33m^* q^2 N_{2d}}{8\hbar^2 \varepsilon_0 \varepsilon_b}\right)^{1/3} \tag{16.74}$$

We also have the definitions for Eq. (16.71):

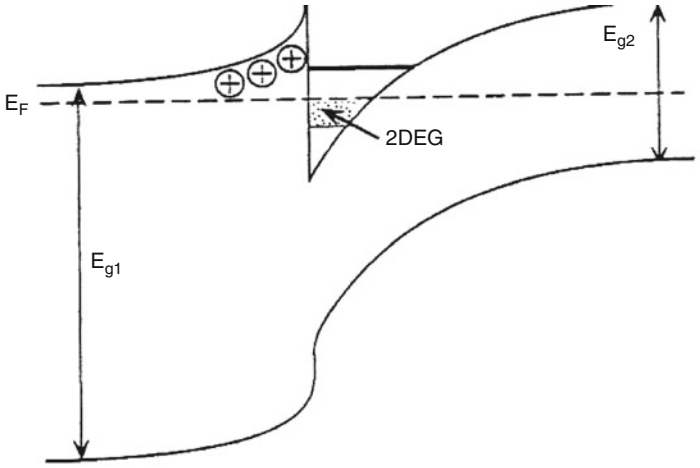

Fig. 16.12 Energy band diagram for a modulation-doped heterostructure (Copyright 1995 from "The MOCVD Challenge Vol. 2, A survey of GaInAsP-GaAs for photonic and electronic device applications," Razeghi, M., p. 371, Fig. 9.2. Reproduced with permission of Routledge/Taylor & Francis Group, LLC)

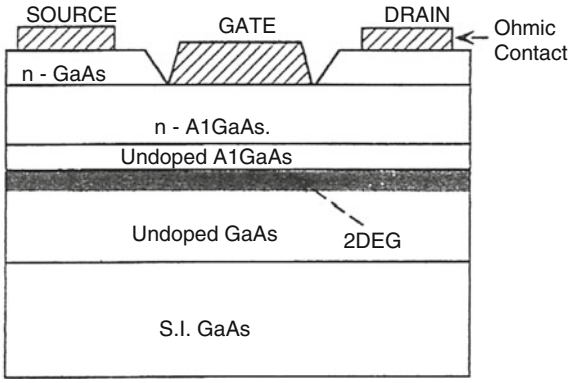

Fig. 16.13 Typical cross section of an AlGaAs/GaAs MODFET (Copyright 1995 from "The MOCVD Challenge Vol. 2, A survey of GaInAsP-GaAs for photonic and electronic device applications," Razeghi, M., p. 372, Fig. 9.3. Reproduced with permission of Routledge/Taylor & Francis Group, LLC)

$$q_I = 2/a_{\mathrm{BI}}$$
$$a_{\mathrm{BI}} = \frac{4\pi\varepsilon\varepsilon_0}{m^* q^2} \tag{16.75}$$

where a_{BI} is the effective radius around the hydrogenic dopant charge. To a reasonably good approximation, the rate can be written in the very simple form:

$$\frac{1}{\tau_{\mathrm{imp}}} = N_{\mathrm{imp}} \frac{\pi\hbar}{8m^*(|d|k_F)^3} \tag{16.76}$$

For a concentration N_{2D}~ 3.10^{15} m^{-2}, $d = 30$ nm and $N_{\text{imp}} = 10^{16}$ m^{-2}, $m = m_0$ The exact result is μ~50m^2/Vs and if this is the dominant source of scattering at low temperatures, the mean-free path is $l_c \sim 5$ μm.

In contrast, the acoustic phonon scattering rate, using the same wavefunctions, can be shown to be using the electron-phonon coupling from Chap. 15:

$$\frac{1}{\tau_{\text{ac}}} = \frac{3m^* bkT(D_{\text{ac}})^2}{16\rho_d v_s^2 \hbar^3} \tag{16.77}$$

The LO optic phonon rates start at higher temperatures when such phonons can be excited as expressed by the Bose distribution function and give:

$$\frac{1}{\tau_{\text{LO}}} = \left(\frac{2m^*\omega_{\text{LO}}}{\hbar}\right)^{1/2} \frac{q^2}{8\hbar\varepsilon_0}\left(\frac{1}{\varepsilon(\infty)} - \frac{1}{\varepsilon(0)}\right)\left(\frac{1}{\exp\left(\frac{\hbar\omega_{\text{LO}}}{k_b T}\right) - 1}\right) \tag{16.78}$$

In GaAs the LO-phonon scattering rate is ~ $\{10^{13}\frac{1}{e^{\hbar\omega_{\text{LO}}/k_b T}-1}\text{Hz}\}$ and therefore very strong and dominant when $T > 40$ K. The temperature structure is very close to what is shown in Figs. 16.11 and 16.14 as one crosses into the temperature region when optic phonons are excited, i.e., $T > 40$ K. Figure 16.12 defines the two-dimensional electron gas referred to as 2DEG, exhibits the difference between the mobility in the bulk and in a 2DEG gas, and shows how the various theoretical scattering mechanisms can explain the temperature behavior in the two systems.

16.1.10 Motion in the Plane: Magnetoresistance and Hall Effect in Two-Dimensional Electron Gas

As a consequence of the high mobilities and long mean free paths, carrier dynamics also exhibit beautiful quantum effects in the presence of an applied magnetic field. We first recall what happens to the spectrum of a 2DEG in a magnetic field from Chap. 4. As we recall from Fig. 4.14 and Eq. (4.174), the magnetic field enhances the Landau level splitting and increases the density of states in each subband, so that as we go up in magnetic field B, the Fermi level is pushed down until at very high B field, only the first subband is occupied. As the Fermi level moves through the Landau levels, one must remember that these have a finite broadening caused by scattering from disorder, and they will typically look like Fig. 16.15 or Fig. 16.16. The localization of eigenstates at the band edges produced by disorder and the Shubnikov-de Haas oscillations in the conductivity and the quantum Hall conductivity derived from the Quantum hall effect (QHE) were discussed briefly and qualitatively in Chap. 15. The objective in this chapter is to introduce the reader also to the new mathematical physics.

Consider first the classical Drude magnetoresistance we derived in Sect. 10.8. This formula was good enough for most optical applications, but it ceases to be

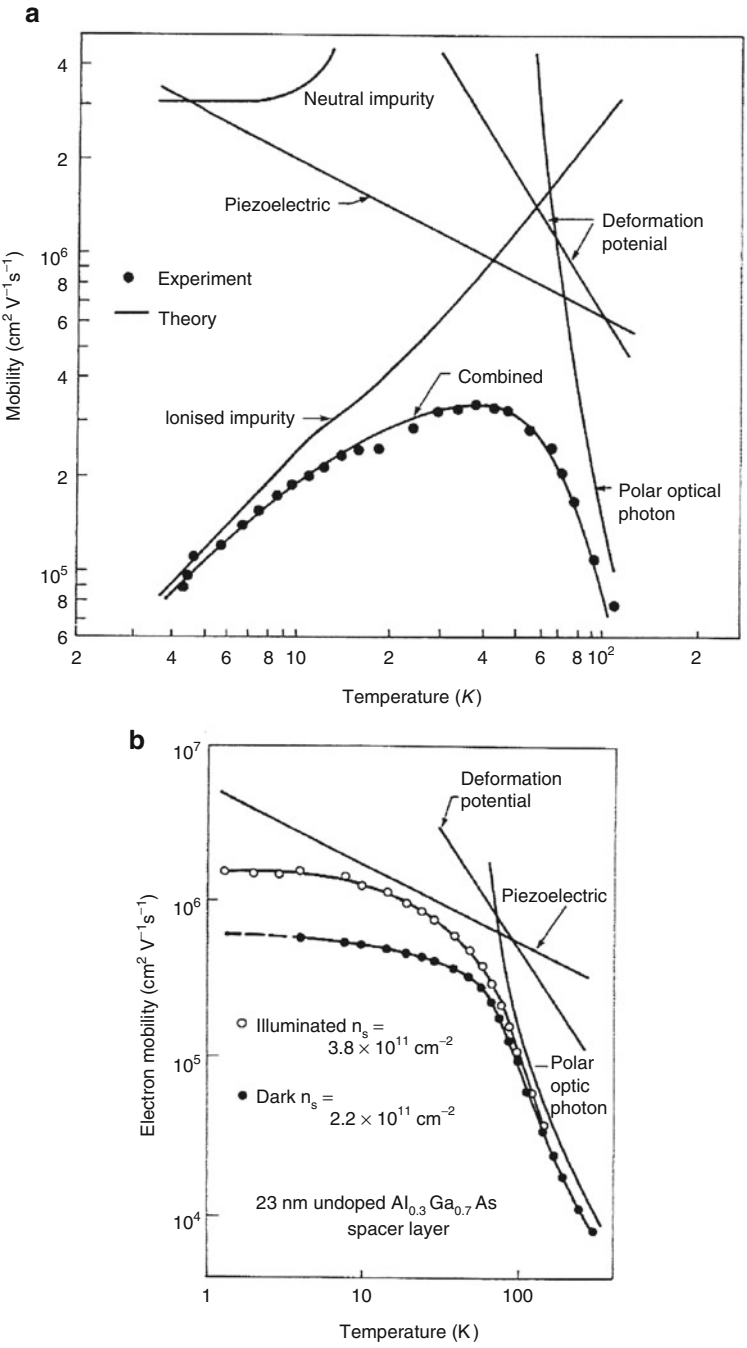

Fig. 16.14 Theoretical and experimental mobility of (**a**) high-purity GaAs (**b**) at a heterojunction. The theoretical lines give the limits placed on the mobility by the relevant scattering mechanisms (Part (**a**) Reprinted with permission from Thin Solid films Vol. 31, G E Stilman and C M Wolfe, "Electrical characterization of thin epitaxial layers" pg. 69 Fig. 7, copyright 1976 Elsevier. Part (**b**) Reprinted with permission from IEEE Tech Digest, International Electron Devices Meeting, Dilorenzo, J., Dingle, R., Feuer, R., Gossard, M., Hendel, A., Hwang, R "Materials and devices Characterization for selectively doped heterojunction transistors," p. 578–581, Fig. 3. Copyright 1982, IEEE, New York)

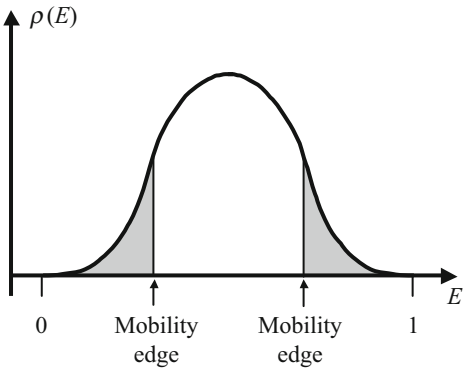

Fig. 16.15 Density of states model of a single Landau level broadened by disorder and showing the shaded region where the eigenstates are expected to be localized. As the Fermi level crosses the density of states, it goes through extended and localized regions. The longitudinal conductivity is zero when the Fermi level is in the localized region, and the Hall conductivity does not change until the Fermi level is again in extended states

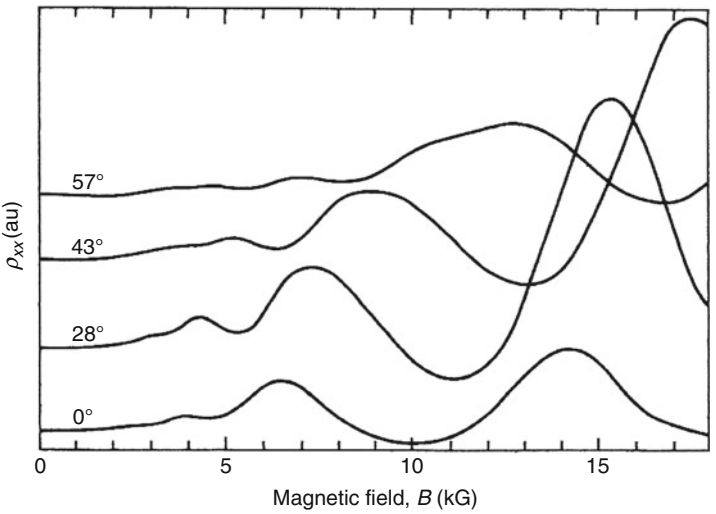

Fig. 16.16 Longitudinal magnetoresistance ρ_{xx} of low-pressure MOCVD-grown GaInAs/InP versus magnetic field for various angles at 4.2 K (Copyright 1989 from "The MOCVD Challenge, Vol. 1: A Survey of GaInAsP-InP for Photonic and Electronic Applications," Razeghi, M., p. 125, Fig. 3.48. Reproduced with permission of Routledge/Taylor & Francis Group, LLC)

useful at high magnetic fields in high mobility 2DEG systems, where Landau levels appear. An improvement which takes the Landau quantization into account and allows also for a lifetime broadening and impurity scattering was derived by Ando et al. (1982). The conductivity becomes in the effective mass approximation:

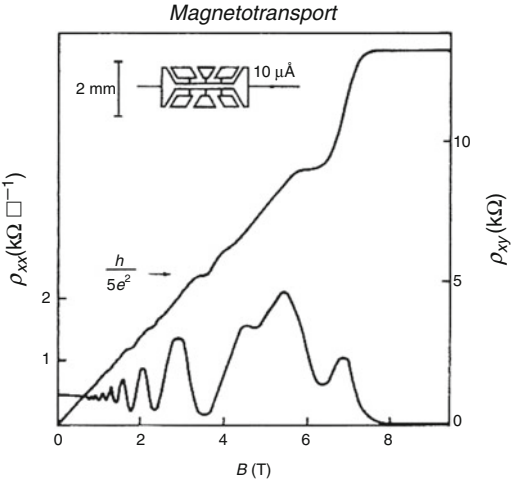

Fig. 16.17 Resistivity data ρ_{xx} and ρ_{xy} at 1.3 K for an InGaAsInP heterostructure (MOCVD) growth technique ($4.3 \times 10^{11}\text{cm}^{-2}$) $\mu = 60000\,\text{cm}^2/\text{V/s}$ (Copyright 1989 from "The MOCVD Challenge, Vol.1:A Survey of GaInAsP-InP for Photonic and Electronic Applications," Razeghi, M., p. 131, Fig. 3.53. Reproduced with permission of Routledge/Taylor & Francis Group, LLC)

$$\sigma_{xx}^{2D}(\omega = 0, B) = \frac{q^2 N_{2D}\tau}{m^*}\frac{1}{1+(\omega_c\tau)^2}\left\{1 - \frac{2(\omega_c\tau)^2}{1+(\omega_c\tau)^2}S(\omega_c)\right\} \tag{16.79}$$

$$S(\omega) = \frac{2\pi^2 k_b T}{\hbar\omega_c}\text{cosech}\left(\frac{2\pi^2 k_b T}{\hbar\omega_c}\right)\cos\left(\frac{2\pi\varepsilon_F}{\hbar\omega_c}\right)\exp\left[-\frac{\pi}{\omega_c\tau}\right] \tag{16.80}$$

when $(\omega_c\tau < 1)$, where τ is the scattering rate ω_c the cyclotron frequency and N_{2D} the carrier density in 2D. The oscillatory structure of this function reproduces the measured structure shown in Figs. 16.16 and 16.17, and indeed it is possible from this comparison to deduce the effective mass and scattering rates (Weisbuch and Vinter 1991).

Now consider the quantum Hall conductivity also shown in Fig. 16.17. In order to fully appreciate the significance of this phenomenon, it is necessary to mentally get rid of the scattering process altogether and consider the pure quantum state with magnetic field B and in the presence of the applied electric field F. The full Hamiltonian in the Landau gauge is:

$$H\Psi = \left\{\frac{1}{2m}(p_y + qxB_z)^2 + \frac{p_x^2}{2m^*} + \frac{p_z^2}{2m^*} + qF_x x\right\}\Psi = E\Psi \tag{16.81}$$

In a 2DEG formed by modulation doping or a quantum well confinement, the motion in the z-direction is bounded, so that the wavefunctions and energies in the z-direction are not free-electron like. But for the present purpose, this is immaterial. We also drop the z-index on the B field. The new electric field-dependent term qFx can be combined into the x-dependent B-terms. The solution is a straightforward extension of the $F = 0$ problem to give:

$$\Psi_n(p_y,p_z) = \left(\frac{1}{L_y L_z}\right)^{1/2} \exp\left[\frac{i}{\hbar}(p_y+p_z)\right]\phi_n\left(x-x_{p_y}\right) \tag{16.82}$$

$$\phi_n(x) = \left(\frac{1}{2^n n!\sqrt{\pi}}\right)^{1/2} \frac{1}{\sqrt{a_0}} \exp\left[-\frac{1}{2}(x/a_0)^2\right] H_n(x/a_0) \tag{16.83}$$

$$a_0 = \left(\frac{\hbar}{m^*\omega_c}\right)^{1/2} \tag{16.84}$$

The energy levels are:

$$E_n(p_y,p_z) = \hbar\omega_c(n+1/2) + qF_x x_{p_y} + p_z^2 + \frac{m^*}{2}(F_x/B)^2 \tag{16.85}$$

$$x_{p_y} = \frac{1}{qB}\left[p_y + m^*\left(\frac{F_x}{B}\right)\right] \tag{16.86}$$

2DEG confinement in the z-direction would replace $p_z^2 \rightarrow E_{z,\mu}$, and these would correspond to the z-eigenvalues of the Fang-Howard model in Eq. (16.73), for example. Note the interesting fact that the energy levels depend on the value of the y-momentum and that the value is asymmetric with p_y, so that the negative p_y will have lower energy, and these eigenstates will be the first to be occupied at $T = 0$. Now consider the quantum current in the y-direction. Remember that the velocity in a magnetic field is different so that the momentum becomes $mv_y = -i\hbar\frac{\partial}{\partial y} \rightarrow -i\hbar\frac{\partial}{\partial y} + qB_z x$, now taking the matrix element of the new operator and then giving a velocity which is remarkably independent of p_y:

$$J_y = -q\sum_{p_y} f(p_y)\frac{1}{B}F_x = -N_{2D}\frac{q}{B}F_x \tag{16.87}$$

The sum over p_y at $T = 0$ just gives the total number of occupied electronic states. Noting that the degeneracy of each Landau level is $\frac{qB}{h}$, so that for i_L number of full bands $N_{2D} = i_L qB/h$, we obtain for the Hall conductivity of electrons:

$$\sigma_{xy} = -q\sum_{p_y} f(p_y)\frac{1}{B} = -i_L\frac{q^2}{h} \tag{16.88}$$

The Hall conductivity is dependent only on the filling index of the Landau subbands i_L. The quantity one normally works with is the Hall resistivity defined as:

$$\rho_{xy} = \frac{\sigma_{xy}}{\sigma_{xy}^2 + \sigma_{xx}^2} \tag{16.89}$$

and the magnetoresistivity is given by:

$$\rho_{xx} = \frac{\sigma_{xx}}{\sigma_{xy}^2 + \sigma_{xx}^2} \tag{16.90}$$

When the Fermi level is in a Landau gap, $\sigma_{xx} = 0$ but σ_{xy} is not, so the magnitude of the Hall resistance is:

$$\rho_{xy} = \frac{1}{i_L}\frac{h}{q^2} \tag{16.91}$$

Now let us look at an experiment. We note that Fig. 16.17 is similar to Fig. 15.20 obtained in a more accurate measurement configuration. It shows that the measured Hall conductivity has plateaus. Every time the Fermi level passes into the edge region where the levels are localized as shown in Fig. 16.15, the Hall resistivity does not change, because localized levels do not conduct. But as soon as we pass the edge of the Landau levels, and reach the middle of the Landau bands where the levels are delocalized, the Hall conductivity changes again, going "up or down" depending on whether we are decreasing or increasing the magnetic field. The Hall resistivity decreases rapidly as we cross the "free" region in the direction of increasing magnetic field B. Now consider the longitudinal resistivity ρ_{xx}. Every time the Fermi level passes through the Landau gaps, we know from Eq. (10.22) in Chap 10 that a null or a localized spectrum implies a zero conductivity and thus from Eq. (16.91) a peak in the resistance. Since a minimum scattering rate finite relaxation time is inevitable, the Ando formula (Eqs. (16.79) and (16.80)) is in practice a good approximation. The remarkable feature of the Hall conductivity is that despite the fact that there are regions of localized states and that electrons that occupy these states do not conduct, the total Hall current behaves as if all the electrons have transported normally as free carriers. The free carriers have acquired a higher velocity which exactly compensates for the ones which are not moving (Prange 1981).

The important point is that the quantum Hall current flows even when the band is full, and the Fermi level is in a mobility gap in the bulk of the sample. It is not a Fermi level property as is ordinary conduction. Indeed when the Fermi level is in a gap, by definition, all the $\{+p_y$ and $-p_y\}$ states from Eq. (16.85) are occupied, and there is no free eigenstate until one goes up to the next Landau level which is a distance $\hbar\omega_c$ away in energy space. The Hall current in a full band is like a diamagnetic current which is associated with an equilibrium state of the system in magnetic field. If one introduced an obstacle in the path of the carriers, the current would flow around the obstacle, and its total value would remain the same (Prange 1981). Carriers cannot be scattered back and redistributed in other locations of space because all the eigenstates are full. If they could, then the eigenstates would be

redistributed or mixed into higher Landau bands, and the Fermi level would not remain in the mobility gap. The system creates new disturbed or scattered eigenstates which are linear combinations of the plane wave states $\exp\left(\frac{ip_y y}{\hbar}\right)$ considered above in Eq. (16.82). Every time $\{+p_y$ and $-p_y\}$ current contributions are added in this admixture, the net current is the same amount as for the undisturbed pairs. If the disturbance is such as to seriously mix the Landau bands, the Landau levels lose their identity, then the Fermi level no longer stays in a mobility gap, and the semiclassical conditions and Hall current are recovered. The same is true if the electron-phonon scattering destroys the quantum coherence of the Landau eigenstates making them so broad that they overlap each other.

16.1.11 The Fractional Quantum Hall Effect

Going back to the Hall experiment reveals that more detail appears in the Hall resistance structure as we go to higher and higher mobility and larger magnetic fields as shown in Fig. 16.18. The additional substructures are believed to be caused by

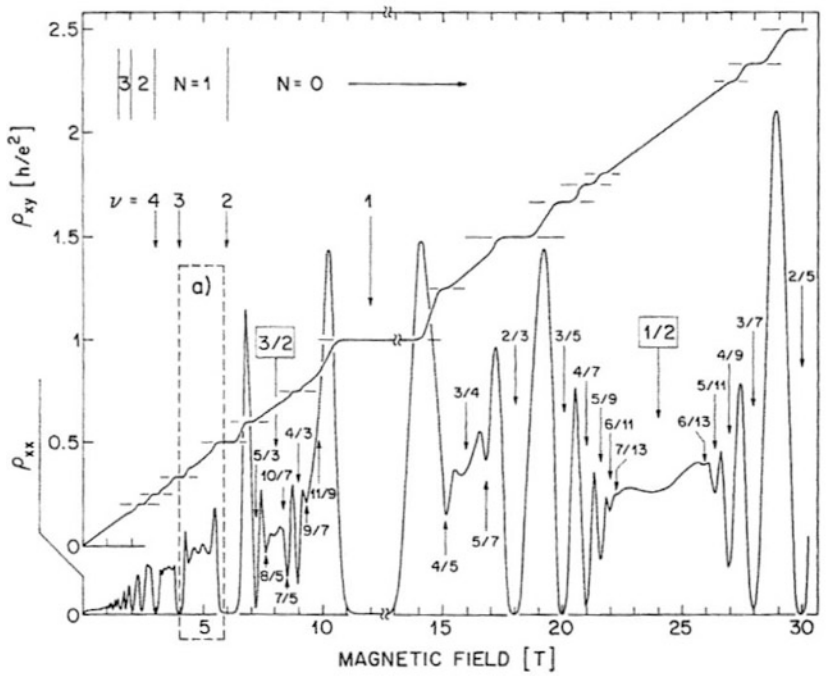

Fig. 16.18 Longitudinal resistivity ρ_{xx} and transverse resistivity ρ_{xy} of a high mobility two-dimensional electron ga at 150mK, showing the fractional quantum Hall effect filling factor ν is indicated and ρ_{xx} is reduced by a factor of 2.5 at high fields. (Reprinted with permission from Physical Review Letters Vol. 59, Willett, R., Eisenstein, H., Stoermer, H., Tsui, D., "Observation of an even denominator quantum number in the Fractional Quantum Hall effect," p. 1776, Fig. 1. Copyright 1987, American Physical Society)

electron-electron interactions. First we recall from Chap. 14 that in a 2DEG the screening is not as effective as in 3D. This is further accentuated by the high magnetic fields which produce gaps in the energy spectra and thus make it more difficult for charges to move and respond to the presence of other charges. In the high mobility 2DEG, we are dealing with mean-free paths of order 10 μm or more. The most serious disturbance seen by an electron in its "magnetic orbit," apart from the edge of the sample, is the presence of other electrons. In the presence of a strong magnetic field, the field caused by the other carrier constitutes a serious disturbance and generates novel forms of many-electron organizations, similar but even more complex than superconductivity. The charges and spins correlate their motion in pairs, threes, and even in lattices. . ., etc., in such a way as to reduce the total potential Coulomb energy. These coupled particles are also called quasi-particles and create their own energy gaps and elementary excitations. The excitations across the many body energy gaps can appear as particles with fractional charges, and this then produces the fractional quantum Hall effect (FQHE) characteristics shown in Fig. 16.18. One can see in this diagram that in addition to the usual Landau bandgaps, the system now exhibits new zeros in its "longitudinal resistivity" as defined by Eq. (16.90) and new plateaus in the "Hall resistivity" (Eq. (16.89)). At low densities, Wigner (1934) has shown that an electron gas prefers to crystallize on a lattice in order to minimize its potential energy. In a so-called Wigner crystal, electronic motion is then similar to phononic vibrations, and the system becomes an insulator. This trend is enhanced by a strong magnetic field which forces the electrons to move in Landau orbits. Now it can happen that for various electron densities or Landau band filling, "partial crystallization" takes place in a magnetic field, which is to say that the electron motions become correlated as described by the Laughlin wavefunction, yet they remain fluid and do not assume a rigid lattice-like correlation of a classic Wigner crystal. Each electron is not shared at a group of sites, and each site now appears to carry a fractional part of the charge. The new electronic "self-organization" is such that at any time, a fraction of the charge builds a Wigner type lattice to lower the Coulomb energy of the electron gas and is consequently immobilized, while the remaining fraction can conduct through the gaps of the Landau-Wigner lattice (fluid), giving the illusion of fractional charges (Laughlin 1983). Localized and mobile charges can exchange places in this highly correlated Wigner-Landau fluid. As in superconductivity, electrons add at one end (input electrode) into the many body collective state and leave at the other end (output) leaving the "many body collective" more or less intact. The charge transfer is in effect therefore the continual reorganization and exchange of particles with a many body state. The detailed discussion of this fascinating topic is however far beyond the scope of this book, and the reader is referred to the original literature on this subject (see Tsui et al. 1983 and Laughlin 1983).

16.1.12 Landau-Stark-Wannier States

The reader should note that we can also solve for the superlattice with an electric field in the growth direction as we did in Sect. 16.1.5 and also now allow a magnetic field in the growth direction (perpendicular to the plane). The combination of electric and magnetic field in the growth direction then generates the so-called Landau-Stark-Wannier bands. The wavefunctions are:

$$\Psi_{n,l,\nu}(p_y;x,y,z) = \left(\frac{1}{L_y}\right)^{1/2} \exp\left[\frac{i}{\hbar}(p_y y + p_z z)\right] \phi_n\left(x - x_{p_y}\right) \frac{1}{\sqrt{c}} J_{\frac{z}{c}-\nu}\left(\frac{2t_l}{qFc}\right) \tag{16.92}$$

$$\phi_n(x) = \left(\frac{1}{2^n n!\sqrt{\pi}}\right)^{1/2} \frac{1}{\sqrt{a_0}} \exp\left[-\frac{1}{2}(x/a_0)^2\right] H_n(x/a_0) \tag{16.93}$$

The energies are p_y, independent as in the 2DEG, and have the same degeneracy per Landau band:

$$E_{n,l,\nu} = \hbar\omega_c(n + 1/2) + qFc\nu + E_l^0 \tag{16.94}$$

where ν is again an integer which ranges from $[-\infty, \infty]$. When the magnetic field is applied in the plane of the superlattice, with an electric field in the growth direction as above, the mathematics is somewhat more complicated but still tractable in terms of the so-called Mathieu functions (Movaghar 1987). The electron moves in Landau orbits which are interrupted by the SL potential. The Landau confinement now competes with the Stark-Wannier localization, producing unusual electron dynamics. Novel effects are expected when the cyclotron radius $l_c = \sqrt{\frac{\hbar}{qB}}$ (see Eq. (10.119)) starts to compete with the Stark-Wannier localization length (Eq. (16.65)). This configuration has not been studied much because of the complexity of the experimental process involved. Applications could be envisaged in the fine-tuning of energy levels and performances of the quantum cascade laser (QCL). However fascinating the physics, applying a magnetic field of 5 T or more changes the size and cost of the device to such an extent that it renders it normally impractical as a "simple" laser system. But recently some workers have indeed made QCL structures which operate in perpendicular to the plane magnetic fields and which show promise as terahertz (THz) photodetectors and terahertz lasers (Scalari et al. 2006).

16.1.13 The Effective Mass of Carriers: Cyclotron Resonance

Using light it is possible to excite carriers from one Landau level to the other. The difference in energy between two adjacent subbands is $h\nu = \hbar\frac{qB}{m^*} \sim 10^{-4} B\frac{m}{m^*}$ eV where B is measured in Tesla. So an absorption experiment in the far infrared and

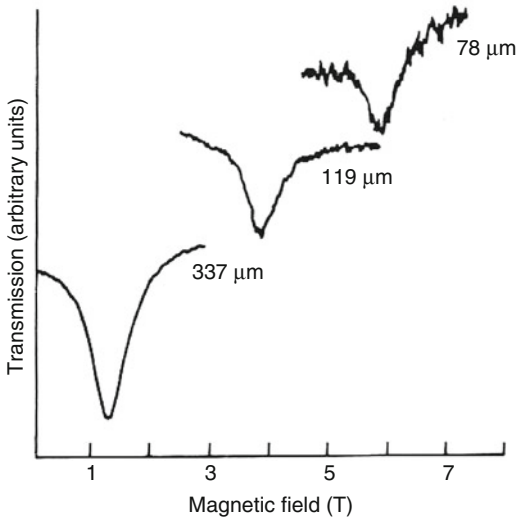

Fig. 16.19 Experimental recording of the transmission of 337, 119, and 78 μm radiation by $Ga_{0.47}In_{0.53}As$ as a function of magnetic field $\mu = 60000 cm^2/V/s$ (Copyright 1989 from "The MOCVD Challenge, Vol. 1: A Survey of GaInAsP-InP for Photonic and Electronic Applications," Razeghi, M., p. 145, Fig. 3.65. Reproduced with permission of Routledge/Taylor & Francis Group, LLC)

at low temperatures should reveal distinct inter-Landau subband absorption processes, and the position of the energy resonance should allow us to deduce the effective mass. This is indeed one of the standard ways of measuring the effective mass, and an example is shown in Fig. 16.19. In materials with small effective mass, it is also possible to use this method to study how the effective mass changes with temperature and magnetic field. The way the change in the effective mass comes about can be seen from the Kane formula for the effective mass as discussed in Chap. 5. Temperature changes the bandgap; it reduces it in most semiconductors because the lattice tends to expand. The change in bandgap is roughly $\sim \gamma_T k_b T$ where the constant γ_T is of order 1 and varies from material to material. The change in bandgap will also according to Eq. (5.82) change the effective mass. However these averaged Kane effective mass corrections are very small, and one has to consider other corrections to the electronic energies as well. For example, one needs to include effects such as electron-phonon scattering and the resulting energy shifts which were briefly considered in Chap. 16. The excitation of phonons with temperature causes disorder, which scatters the electrons, and this gives rise to energy shifts which are corrections and appear as temperature-dependent energies, effective masses, and lifetimes. Though interesting and important, these corrections are second-order effects. They are important in low bandgap and small effective mass materials, such as InSb, but they constitute a specialized subject which is beyond the scope of this book.

16.1.14 Summary

In this chapter we introduced the reader to the way one would calculate electrical conduction using quantum mechanical methods. We used a simple example of a

structure one could engineer using modern growth techniques and worked it through. The generalization to more complex systems is in principle then straightforward. We explained how one can, when appropriate, relate quantum transport to the classical Drude method. We introduced also the double barrier system and explained how one can have a negative resistance and engineer the so-called negative differential resistance (NDR) device. The effect of a magnetic field perpendicular to the plane of motion in a two-dimensional electron gas (2DEG) was also considered. We showed how the Landau levels give rise to "Shubnikov de Haas" oscillations in the conductivity and the quantum Hall effect. Finally we studied what would happen to a carrier which is in a narrow band under the influence of an electric field. We derived the Stark-Wannier (SW) states and introduced the student to the fascinating new physics that this involves. This new physics is now realizable with semiconductor molecular beam epitaxy (MBE) and metalorganic chemical vapor deposition (MOCVD) growth techniques.

16.2 Electron-Phonon Interactions

16.2.1 Introduction

In Sect. 16.2.1 we treated electrical transport. There we made the observation that one of the reasons why carriers scatter and lose momentum is because they interact with the lattice vibrations, and this causes them to either gain or lose energy. Such processes, during which energy is exchanged, are called "inelastic scattering" processes. But electron-lattice interactions do much more than just cause resistance. They are also at the origin of such phenomena as superconductivity where phonons help two electrons (fermions) to bind together to form bosons (integer spin particles) which can condense into superfluids. But we will not go as far as that in this book and focus on some very elementary properties of electron-phonon coupling mainly the ones which enter transport properties.

Let us now look at the structure of the electron-lattice interaction, this coupling is also called the electron-phonon interaction. The reason for such a coupling is that when atoms move around, vibrate, and oscillate, they no longer form perfectly periodic arrays of potentials. But the electron Bloch functions were derived under the assumption that the system is at $T = 0$ and that the lattice is perfectly periodic. So these deviations from periodicity caused by thermal excitations cause a perturbation on the electron motion in Bloch bands; this causes them to scatter from one Bloch state k to another Bloch state k', exchanging momentum and energy in the process. The momentum difference is supplied by the lattice waves or, in quantized form, by the "phonons." One assumption which facilitates the analysis is the so-called Born-Oppenheimer approximation. This approximation is based on the observation that the electronic motion is very much faster than the lattice atom motion, the time scales being $\sim 10^{14}$ Hz (electron bandwidth) compared to 10^{12} Hz (lattice vibrational frequency at the Debye value), respectively. This implies that in most solids of interest to us, the electrons, when they move, see a more or less frozen lattice and

have time to build new eigenstates before the atom configurations change substantially. So the electrons form their new disturbed energy bands before the lattice has had time to change; this happens at least after the unit of time for the lattice, which is a lattice vibration. When the lattice configuration changes, the electrons respond by transferring to the new energy states formed by the new lattice configuration while conserving the total energy. This observation is also the basis for the methods used to perform numerical simulations of electron-phonon coupling in solids. One starts from a given lattice configuration, then solves for the electron energy levels, then allows a new configuration to evolve which obeys the lattice dynamics which can be assumed to obey Newton's laws. Then one solves again for the electron states, under the assumption that the new eigenstates obey trajectories which have the same total energy, vibrational and electronic. Numerical solutions of coupled electron-lattice systems are computationally very challenging and in their infancy. Fortunately, exact solutions are easier in nanoparticles and nanostructures where they are also more needed and much more relevant.

Now consider the formal derivation of the coupling with the help of which we can study the scattering rates using perturbation theory. We write for the electron ion interaction as usual:

$$H_{\text{el-ion}} = \sum_{l} V_{\text{el-ion}}\left(\vec{r} - \vec{R}_l\right) \tag{16.95}$$

Allowing the atomic variables $\vec{R}$, where $\vec{r}$ is the electron position, to deviate slightly from their equilibrium positions permits us to write the Hamiltonian in terms of one which describes the equilibrium periodic position and a nonperiodic term which scatters the electrons:

$$H_{\text{el-ion}} = H^0_{\text{el-ion}} + H_{\text{el-ph}} \tag{16.96}$$

Allowing the deviations from equilibrium of the α_{th} atom in the n_{th} Wigner-Seitz cell to be called $u_{n,\alpha}\left(\vec{R}\right)$, we can write:

$$V\left(\vec{r} - \vec{R}_{n\alpha} - \vec{u}_{n\alpha}\right) = V_\alpha\left(\vec{r} - \vec{R}_{n\alpha}\right) - \vec{u}_{n\alpha} \cdot \vec{\nabla}\, V_\alpha\left(\vec{r} - \vec{R}_{n\alpha}\right) \tag{16.97}$$

Now we note that the atomic deviation from equilibrium can be expanded in terms of the normal coordinates. The momentum index $\vec{q}$ should not be confused with the charge q:

$$\vec{u}_\alpha\left(\vec{R}\right) = \frac{1}{\sqrt{NM_\alpha}} \sum_{\vec{q}} Q_{\vec{q}}\, \vec{e}_{\alpha,\vec{q}}\, \exp\left[i\, \vec{q} \cdot \vec{R}\right] \tag{16.98}$$

where $\vec{e}_{\alpha,\vec{q}}$ is the polarization of the vibrational motion of the α_{th} atom in the q_{th} mode at the $\boldsymbol{R}$ site and M_s is the ionic masses. We can write the coupling as:

$$H_{\text{el-ph}} = -\sum_{\alpha,n} \frac{1}{\sqrt{NM_\alpha}} \sum_{\vec{q}} Q_{\vec{q}} \vec{e}_{\alpha,\vec{q}} \exp\left[i\,\vec{q}\cdot\vec{R}_n\right]\cdot\vec{\nabla}\, V_\alpha\left(\vec{r}-\vec{R}_{n\alpha}\right) \tag{16.99}$$

The adiabatic or Born-Oppenheimer approximation stipulates that one can write the total wavefunction as a product of electron and phonon wavefunctions so that:

$$\Psi_{\text{total}} = \Psi\left(\vec{r},\vec{R}\right)\Phi\left(\vec{R}\right) \tag{16.100}$$

where Φ is the wavefunction of all the ions and $\Psi\left(\vec{r},\vec{R}\right)$ is the wavefunction of the electrons in the instantaneous potential of the ions. When the ions move, the potential changes as they move, and we have a time evolving Hamiltonian where the electron potential at any time depends on the instantaneous position of the ions and trajectories conserve total energy. The motion of the ions was treated in Sect. 16.2.1 using classical mechanics. In principle the ions obey also the Schrödinger equation (see Eq. (4.8)) which can be written as:

$$H_{\text{ions}} = \sum_l \frac{p_l^2}{2M_l} + \sum_{l,m} K_{l,m}\left(\vec{R}_m - \vec{R}_l\right)\vec{u}_l\vec{u}_m + H_{\text{nonl}} \tag{16.101a}$$

where $\vec{u}_s$ are the displacements from equilibrium, p_l is the ionic momentum operator, $K_{l,m}$ is the restoring force per unit displacement, and H_{nonl} is the nonlinear term which is due to anharmonic forces (higher powers in u). It was shown in Chap. 6 that in the harmonic approximation, the lattice waves propagate as harmonic plane waves with solutions of the type:

$$\vec{u}\left(\vec{k},\omega\right) = \vec{u}_0 \exp\left[i\left(\vec{k}\cdot\vec{r}-\omega t\right)\right] \tag{16.101b}$$

with acoustic and optic branch frequency dispersions $\omega_{\vec{q},b}$ as shown in Chap. 6 and where b denotes the branch. We then assumed that in quantum mechanics, the lattice vibrations become quantized and can be thought of as particles with energies $\hbar\omega_{\vec{q},b}$, the so-called phonons. In quantum mechanics, and in the harmonic approximation, the solutions of Eq. (16.101) are the Bloch version of the localized harmonic oscillator wavefunctions.

In quantum mechanics, we note that the total wavefunction which describes the noninteracting unperturbed electron gas and the unperturbed phonon system, or lattice vibrations system, can be written as a product of the two wavefunctions:

$$\Psi = \Psi_{n\vec{k}}\left\{\phi_{\vec{q}_1},b\phi_{\vec{q}_2},b\ldots\ldots\phi_{\vec{q}_N},b\right\} \tag{16.102}$$

where $\psi_{\mathbf{nk}}$ is the electron state in the band index n and $\phi_{\vec{q},b}\left(\vec{R}_1,\vec{R}_2,\ldots\vec{R}_N\right)$ the wavefunction of a phonon with momentum index $\vec{q}$ in the b-branch (acoustic or

optic). We abbreviate the collective set of atomic displacements by the symbol $\vec{\Omega}$ so that the matrix element between two states ϕ, ϕ' which differ by the occupation of one phonon mode, abbreviated by n, becomes:

$$\begin{aligned}\int d\Omega_{\vec{q},b}\phi_{\vec{q}'',b}(\vec{Q})Q_{\vec{q},b'}\phi_{\vec{q}',b''}(\vec{Q}) = &\left(\frac{\hbar}{2\omega_{\vec{q},b}}\right)^{1/2}\delta_{\vec{q},\vec{q}',\vec{q}''}\delta_{b,b',b''}\\ &\times\left\{\left(n_{q,b}(\omega_{q,b})\right)^{1/2}\delta_{n',n-1}\right.\\ &\left.+\left(1+n_{q,b}(\omega_{q,b})\right)^{1/2}\delta_{n',n+1}\right.\end{aligned} \tag{16.103}$$

where the $n_{\vec{k},b}$ is the phonon occupation probability of the $(\vec{k},b)$ mode and for which the thermodynamic average is:

$$< n_{\vec{k},b} >= \frac{1}{e^{\hbar\omega_{\vec{k},b}/kT}-1} \tag{16.104}$$

It is convenient to use the shorthand Dirac notation to denote the phonon wavefunction (one branch only for simplicity):

$$\Psi_{n,\vec{k}}\Pi\phi_{q,b}\ldots\phi_{q,b} = \Psi_{n,\vec{k}}\left|n_{q_1,b}\vec{q}_1,b;n_{q_2,b}\vec{q}_2,b;\ldots;n_{q_N,b}\vec{q}_N,b\right\rangle \tag{16.105}$$

where there are $n_{q,\,b}$ phonons in the state $(q,b)\ldots$, etc. Of course one can use the Dirac notation for electrons too by replacing $\Psi_{n,\vec{k}} \rightarrow \left|(n,\vec{k})\right\rangle_e$ so that:

$$\Psi_{n,\vec{k}}\Pi\phi_{q,b}\ldots\phi_{q,b} = \left|n,\vec{k}\right\rangle_e\left|n_{q_1,b}\vec{q}_1,b;n_{q_2,b}\vec{q}_2,b;\ldots;n_{q_N,b}\vec{q}_N,b\right\rangle_{\text{ph}} \tag{16.106}$$

Then one can write the normal coordinates as operators which act on the Dirac state, and this is called the method of second quantization:

$$Q_{\vec{q},b} = \left(\frac{\hbar}{\omega_{q,b}}\right)^{1/2}\left(a^{+}_{-\vec{q},b}+a_{\vec{q},b}\right) \tag{16.107}$$

such that the operator $a_{\vec{q},b}$ removes a phonon from the state $(\vec{q},b)$ and $a^{+}_{\vec{q},b}$ adds a phonon $(\vec{q},b)$, for example:

$$\begin{aligned}&a^{+}_{q_s,b}\left|n_{q_1,b}\vec{q}_1,b;n_{q_2,b}\vec{q}_2,b;\ldots;n_{q_N,b}\vec{q}_N,b\right\rangle\\ &=\left|n_{q_1,b}\vec{q}_1,b;\left(n_{q_s,b}+1\right)\vec{q}_s,b;\ldots;n_{q_N,b}\vec{q}_N,b\right\rangle\end{aligned} \tag{16.108}$$

$$a_{q_s,b}\left|n_{q_1,b}\vec{q}_1,b;n_{q_2,b}\vec{q}_2,b;\ldots;n_{q_N,b}\vec{q}_N,b\right\rangle = \left|n_{q_1,b}\vec{q}_1,b;\left(n_{q_s,b}-1\right)\vec{q}_s,b;\ldots;n_{q_N,b}\vec{q}_N,b\right\rangle \tag{16.109}$$

Now the electron-phonon interaction can be written in the much more elegant form using the above creation and annihilation operators defined in Eq. (16.108) as:

$$H_{\text{el-ph}} = -\sum_{\alpha,n}\frac{1}{\sqrt{NM_\alpha}}\sum_{\vec{q}}\left(\frac{\hbar}{\omega_{q,b}}\right)^{1/2}\left[a^+_{-q,b}+a_{\vec{q},b}\right]\underset{\alpha,\vec{q}}{\vec{e}}\exp\left[i\vec{q}\cdot\underset{n}{\vec{R}}\right]\cdot\nabla V_\alpha\left(\vec{r}-\underset{n\alpha}{\vec{R}}\right) \tag{16.110}$$

When this operator acts on an electron-phonon basis state of the type (Eq. (15.108)), it raises and lowers the corresponding phonon occupation, and the r dependent terms act on the electron part of the wavefunction. The interaction with the longitudinal optical modes in a semiconductor are most important and take on the simple form (Note: q is charge):

$$H_{\text{el-ph,Lo}} = i\left\{\frac{q^2\hbar\omega_{Lo}}{2\varepsilon_0\Omega^{1/2}}\left[\frac{1}{\varepsilon(\infty)}-\frac{1}{\varepsilon(0)}\right]\right\}^{1/2}\sum_{\vec{k}}\left(\frac{1}{k}\right)\left[-a_k^+\exp\left[-i\vec{k}\cdot\vec{r}\right]+a_k\exp\left(i\vec{k}\cdot\vec{r}\right)\right] \tag{16.111}$$

where $\varepsilon(\infty)$, $\varepsilon(0)$ are the high and zero frequency permittivities and ω_{LO} the LO optical phonon frequency and Ω is the volume. The coupling with the acoustic mode gives:

$$H_{\text{el-ph, ac}} = \sum_{\vec{k}}\left(\frac{\hbar k}{2\Omega\rho_d v_s}\right)^{1/2} iD_{\text{ac}}\left[-a_k^+\exp\left(-i\vec{k}\cdot\vec{r}\right)+a_k\exp\left(i\vec{k}\cdot\vec{r}\right)\right] \tag{16.112}$$

where v_{s} is the velocity of sound, ρ_d the density, and D_{ac} is called the deformation potential.

Alternatively one can avoid the use of creation and annihilation operators and think of the electron-phonon interaction as a time-dependent perturbation of the lattice vibrations on the electron system, so that Eq. (16.65) is also:

$$H_{\text{el-ph, ac}} = \sum_{\vec{k}}\left(\frac{\hbar k}{2\Omega\rho_d v_s}\right)^{1/2} iD_{\text{ac}}\left[-e^{i\omega_{\vec{k}}t}\exp\left(-i\vec{k}\cdot\vec{r}\right)+e^{-i\omega_{\vec{k}}t}\exp\left(i\vec{k}\cdot\vec{r}\right)\right] \tag{16.113}$$

Consider the first-order scattering of Bloch electrons by acoustic phonons using the Fermi golden rule (Eq. (10.65)). The result is for an electron scattering process from k to k' with phonon emission:

$$\frac{1}{\tau_{\text{ac}}\left(\vec{k},\vec{k'}\right)} = \frac{2\pi}{\hbar}\sum_{\vec{k''}}\left(< n_{\vec{k''},\text{ac}} > +1\right) \times \frac{\hbar k''}{2\Omega\rho_d v_s} D_{\text{ac}}^2 \delta_{\vec{k}-\vec{k''},\vec{k'}} \delta\left(\varepsilon\left(\vec{k}-\vec{k''}\right) - \varepsilon\left(\vec{k}\right) + \hbar\omega_{\text{ac}}\left(\vec{k''}\right)\right) \tag{16.114}$$

Initial state was $\left|\vec{k}\right\rangle_{\text{el}} \left|n_{k''}\ldots\right\rangle_{\text{phon}}$ and final state $\left|\vec{k'}\right\rangle_{\text{el}} \left|n_{\vec{k''}}.+1,..\right\rangle_{\text{phon}}$. And for absorption we find:

$$\frac{1}{\tau_{\text{ac}}\left(\vec{k},\vec{k'}\right)} = \frac{2\pi}{\hbar}\sum_{\vec{k''}} < n_{\vec{k''},\text{ac}} > \frac{\hbar k''}{2\Omega\rho_d v_s} D_{\text{ac}}^2 \delta_{\vec{k}+\vec{k''},\vec{k'}} \delta\left(\varepsilon\left(\vec{k}+\vec{k''}\right) - \varepsilon\left(\vec{k}\right) - \hbar\omega_{\text{ac}}\left(\vec{k''}\right)\right) \tag{16.115}$$

Note that when evaluating the matrix elements, we have products and answers of the form ${}_{\text{phon}}\left\langle .n_{\vec{k}},\vec{k}\,..\left|a_{\vec{k}}^{+}a_{\vec{k}}\right|.\ldots.n_{\vec{k}},\vec{k}\right\rangle_{\text{phon}} = n_{\vec{k}}$ and ${}_{\text{phon}}\left\langle .n_{\vec{k}},\vec{k}\,..\left|a_{\vec{k}}a_{\vec{k}}^{+}\right|.\ldots.n_{\vec{k}},\vec{k}\right\rangle_{\text{phon}} = \left(1+n_{\vec{k}}\right)$

The sum over $\vec{q}$ can be transformed into an integral using:

$$\sum_{\vec{q}} \to \frac{\Omega}{(2\pi)^3}\int d\,\vec{q} \tag{16.116}$$

At high temperatures we also have the approximation:

$$< n_{\vec{k},b} > = \frac{1}{e^{\hbar\omega_{\vec{k},b}/kT} - 1} \sim < n_{\vec{k},b} > +1 \tilde{} kT/\hbar\omega_{\vec{k},b} \tag{16.117}$$

so that Eq. (16.105) reduce to the simple form:

$$\frac{1}{\tau_{\text{ac}}\left(\vec{K}\right)}_{\vec{k}-\vec{k'}=\vec{K}} = \frac{2\pi}{\hbar}\frac{k_B T}{\rho_d v_s^2} D_{\text{ac}}^2 g_V\left[\varepsilon\left(\vec{K}\right)\right] \tag{16.118}$$

where $g_V\left(\varepsilon\left(\vec{K}\right)\right)$ is the density of states per unit volume at energy $\varepsilon\left(\vec{K}\right)$. The scattering rate is straightforward to evaluate for optic modes too, and the formulae

can also be easily applied to allow for interband and intersubband scattering in quantum wells.

If we wish to avoid dealing with the creation and annihilation operators and phonon wavefunctions explicitly altogether and use the time-dependent perturbation form (Eq. (16.20)) of the interaction, then we have to put in the phonon probability factor by hand for phonon emission and absorption.

16.2.2 The Polaron Effective Mass and Energy

One of the novel feature introduced by the electron-phonon coupling is the polaron. The polaron is the electron surrounded by its polarization cloud. This polarization cloud is produced around it as a result of the coupling with the lattice. One can look at it this way: the electron has an electric field. This electric field will pull the positive ions toward the electron as it moves around. But moving the lattice ions generates a polarization, and this has dipole moment which couples to the electric field of the electron. The induced polarization couples with charge, and this produces a negative energy shift called polaron energy. As it moves, the electron drags this polarization cloud with itself, and this tends to make it look heavier. In other words, it acquires a polaron effective mass. To calculate this effect, one has to evaluate the second-order perturbation theory energy shift caused by, for example, the optic mode coupling given by Eq. (16.18). This is quite straightforward using Eq. (4.60) from Chap. 4, but it involves some integration. The result is that the electron acquires a new effective mass given by:

$$m^{**} = \frac{m^*}{1 - \alpha_{\text{ep}}/6} \tag{16.119}$$

where (q is the charge):

$$\alpha_{\text{ep}} = \frac{q^2}{8\pi\varepsilon_0\hbar\omega_{oL}}\left(\frac{2m^*\omega_{oL}}{\hbar}\right)^{1/2}\left[\frac{1}{\varepsilon(\infty)} - \frac{1}{\varepsilon(0)}\right] \tag{16.120}$$

The constant entering Eq. (16.110) is tabulated in data banks for semiconductors. Typically the value of α_{ep} is ~0.08 for InP and 0.015 for InSb but as high as ~2.4 and 6.6 for LiI and RbBr, respectively. In highly polar substances, the perturbation method is no longer valid and Eq. (16.10) is not meaningful.

For weak coupling, the other lattice modes also give terms of similar structures, so that the typical increase of the effective mass is never less than a few percent for most semiconductors. There is, as we have observed, also a concomitant energy shift (lowering) caused by the lattice polarization. The energy shift is of the form:

$$\Delta E_{\text{polaron}} \sim -\alpha_{\text{ep}}\hbar\omega_{\text{oL}} \tag{16.121}$$

Thus, typically, GaAs polaron shifts are ~3 meV. The polaron energy shift becomes more pronounced the more confined the electron eigenstate is. Thus in a quantum well or quantum dot, the energy lowering will be bigger, reaching values ~20 meV in GaAs compounds. A more confined electron spends its time visiting on average fewer sites and bonds, and thus has a greater effect on its environment than a highly delocalized charge.

16.2.3 Summary

In this chapter, which concludes the description of transport in solids, we allowed the lattice atoms to move and therefore to produce deviations from pure Bloch symmetry. The self-motion of the lattice produced by temperature, in other words, thermal excitation of phonons, then gives rise to electron-phonon interactions. We derived the optic and acoustic coupling and gave a simple example on how to calculate the electron-acoustic phonon scattering relaxation time. In most crystalline metals and semiconductors, it is the e-phonon scattering which limits the resistance of the material and is even invoked as an explanation of superconductivity. We also introduced the reader to the concept of the polaron and showed how to estimate energy and effective mass shifts in the presence of longitudinal optic mode coupling. We have here given the reader only a very brief description of this very important interaction mechanism and refer the reader to the specialized literature .

Problems for Quantum Transport

1. An electron beam is incident on a barrier where the barrier height is equal to the electron energy and is 8 eV. The transmission coefficient is given by $T = 10^{-3}$, what is the width of the barrier?
2. Calculate the transmission coefficient for the structure depicted in Fig. 16.1 but this time for a well with potential energy $\{-V\}$.
3. Calculate the expectation value of the velocity in the y-direction for an electron in a 2DEG (drop the z-part of the wavefunction) in the presence of a magnetic field perpendicular to the pane and an electric field in the x-direction. (See Eq. (16.82)). If the total number of electrons per unit area is Ns, what is the total current in the y-direction as a function of electric field and magnetic field?
4. Describe the various mechanisms that reduce the mobility in a 2DEG and how they affect the mobility in the different temperature regions. What would happen if one could suppress the optic phonon scattering?

Problems for Electron-Phonon Interactions

1. Why do lattice vibrations cause electrical resistance? In an electronic scattering process, what is the difference between phonon emission and phonon absorption? Using the electron-acoustic phonon interaction from Eq. (16.20) and the Fermi golden rule from Chap. 10, derive the scattering rates given by Eqs. (16.21) and (16.22).
2. Explain what is meant by the electron-phonon interaction. Taking the one-dimensional diatomic chain treated in Chap. 6 as an example, illustrate with a simple diagram the difference between the coupling of an electron to an acoustic and an optic vibration of the chain. It is helpful to think of the electronic bands as overlapping atomic wavefunctions, i.e., to think with the "tight-binding model" of the electronic band structure.
3. In analogy to Eqs. (16.21) and (16.22), write down an expression for the "Fermi golden rule" relaxation rate (see Sect. 16.2.1) of free electrons when they scatter with optic phonons. Consider both phonon emission and absorption. Take the electron wavefunctions to be plane waves.
4. What are the factors which influence the magnitude of the polaron energy shift in a solid (look at Eqs. (16.110) and (16.111))? What materials would you use to make strongly polaronic semiconductors?

References

Ando T, Fowler AB, Stern F (1982) Electronic properties of two-dimensional systems. Rev Mod Phys 54:437

Davies JH (2000) The physics of low dimensional semiconductors. Cambridge University Press, Cambridge

Faist J, Capasso F, Sivco DL, Sirtori C, Hutchinson AL, Cho AY (1994) Quantum cascade laser. Science 264:553

Laughlin RB (1983) The fractional quantum Hall effect. Phys Rev Lett 50:1395

Movaghar B (1987) Theory of high field transport in semiconductor superlattice structures. Semicond Sci Technol 2:185

Prange RE (1981) Quantized Hall resistance and the measurement of the fine-structure constant. Phys Rev B 23:4802

Razeghi M (1989) MOCVD challenge vol.1 a survey of GaInAsP-InP for photonic and electronic applications. Adam Hilger, Bristol

Razeghi M, Tardella A, Davis RA, Long AP, Kelly MJ (1987) Negative differential resistance at room temperature from resonant tunneling GaInAS/InP double barrier structures. IEEE Electron Lett 23:116

Scalari G, Graf M, Hofstetter D, Faist J, Beere JH, Ritchie D (2006) A Thz quantum cascade detector in a strong perpendicular magnetic field. Semicond Sci Technol 21:1743

Slivken S, Evans A, David J, Razeghi M (2002) High average power high duty cycle quantum cascade laser. Appl Phys Lett 81:4321

Tsui DC, Stoermer HL, Hwang JC, Brooks JS, Naughton MJ (1983) The fractional quantum Hall effect. Phys Rev B 28:2274

Wigner EP (1934) On the interaction of electrons in metals. Phys Rev 46:1002

Further Reading

Ahmed H (1986) An integration microfabrication system for low dimensional structures and devices. In: Kelly MJ, Weisbuch C (eds) The physics and fabrication of microstructures and microdevices. Springer, Berlin, pp 435–442

Asada M, Miyamoto Y, Suematsu Y (1986) Gain and the threshold of 3-dimensional quantum-box lasers. IEEE J Quantum Electron 22:1915–1921

Ashcroft NW, Mermin ND (1976) Solid state physics. Holt, Rinehart and Winston, New York

Bastard G (1988) Wave mechanics applied to semiconductor heterostructures. Halsted Press, New York

Beaumont SP (1992) Quantum wires and dots-defect related effects. Physica Scripta 1992 (T45):196–199

Bockrath M, Cobden DH, Lu J, Rinzler AG, Smalley RE, Balents L, McEuen PL (1999) Luttinger liquid behaviour in carbon nanotubes. Lett Nat 397:598–601

Chuang SL (1995) Physics of optoelectronic devices. Wiley, New York

Cochran W (1973) The dynamics of atoms in crystals. Edward Arnold Limited, London

Cohen MM (1972) Introduction to the quantum theory of semiconductors. Gordon and Breach, New York

Dingle R (1975) Confined carrier quantum states in ultrathin semiconductor heterostructures. In: Queisser HJ (ed) Feskoerperprobleme XV. Springer, pp 21–48

Dingle R, Wiegmann W, Henry CH (1974) Quantum states of confined carriers in very thin $Al_xGa_{1-x}As$-GaAs- $Al_xGa_{1-x}As$ heterostructures. Phys Rev Lett 33:827–830

Einspruch NG, Frensley WR (1994) Heterostructures and quantum devices. Academic Press Limited, London

Ferry DK (1991) Semiconductors. Macmillan, New York

Hasko DG, Potts A, Cleaver JR, Smith C, Ahmed H (1988) Fabrication of sub-micrometer free standing single crystal GaAs and Si structures for quantum transport studies. J Vac Sci Technol B 6:1849–1851

Ibach H, Lüth H (1990) Solid-state physics: an introduction to theory and experiment. Springer, New York

Kasap SO (1997) Principles of engineering materials and devices. McGraw-Hill, New York

Kelly MJ (1995) Low-dimensional semiconductors: materials, physics, technology, devices. Oxford University Press, New York

Kittel C (1976) Introduction to solid state physics. Wiley, New York

Maxwell JC (1952) Matter and motion. Dover, New York

Peyghambarian N, Koch SW, Mysyrowicz A (1993) Introduction to semiconductor optics. Prentice-Hall, Englewood Cliffs

Razeghi M, Duchemin JP, Portal JC, Dmowski L, Remeni G, Nicolas RJ, Briggs A (1986) First observation of the quantum Hall effect in a $Ga_{0.47}In_{0.53}As$-InP heterostructure with three electric subbands. Appl Phys Lett 48:712–715

Reissland JA (1973) Physics of phonons. Wiley, London

Rosencher E, Vinter B (2002) Optoelectronics. Cambridge University Press, Cambridge

Sapoval B, Hermann C (1995) Physics of semiconductors. Springer, New York

Scherer A, Jewell J, Lee YH, Harbison J, Florez LT (1989) Fabrication of microlasers and microresonator optical switches. Appl Phys Lett 55:2724–2726

Sze S (1981) Physics of semiconductor devices, 2nd edn. Wiley, New York

Tewordt M, Law V, Kelly M, Newbury R, Pepper M, Peacock C (1990) Direct experimental determination of the tunneling time and transmission probability of electrons through a resonant tunneling system. J Phys Condens Matter 2:896–899

Weiner JS, Miller DAB, Chemla DJ, Damen TC, Burrus CA, Wood TH, Gossard AC, Wiegmann W (1985) Strong polarization sensitive electroabsorption in GaAs/AlGaAs quantum well waveguides. Appl Phys Lett 47:1148–1151

Weisbuch C, Vinter B (1991) Quantum semiconductor structures fundamentals and applications. Academic Press Inc Harcourt Brace Jovanovich, Publishers, Boston